



**University  
of Basel**

# **Graph Denoising for Molecular Imaging**

Master's Thesis

Natural Science Faculty of the University of Basel  
Department of Mathematics and Computer Science  
Signals and Data Group

Examiner: Prof. Dr. Ivan Dokmanić  
Supervisor: Dr. Valentin Debarnot

Cédric Mendelin  
[cedric.mendelin@stud.unibas.ch](mailto:cedric.mendelin@stud.unibas.ch)  
2014-469-274

12.06.2022

## **Acknowledgments**

I would like to express my deepest appreciation to Prof. Dr. Ivan Dokmanić, for giving me the opportunity to conduct my Master's Thesis in the Signals and Data Group.

Further, I am extremely grateful for the support from my supervisors Dr. Valentin Debarnot and Cheng Shi. We had inspiring discussions throughout the project and their valuable feedback was more than welcome, helping me to finish my Thesis in adequate quality.

Many thanks to Patrick Arnold and Marc Hennemann for proofreading this report, their feedback was greatly appreciated.

Words cannot express my gratitude to my wife Luana, my family and friends, for the support during the last years. This accomplishment would not have been possible without them.

## Abstract

In molecular imaging methods Cryo-Electron Microscopy (Cryo-EM) and Computed Tomography (CT) observations are collected from a biological sample. Cryo-EM enables the view of molecules in near-atomic resolution and, therefore, has received a lot of attention in recent years. The Application of Cryo-EM is a major motivation for this Thesis. Observations are noisy due to the imaging process and reconstruction from noisy observations is desired. Reconstruction is challenging due to dealing with enormous noise and unknown observation angles. Moreover, Cryo-EM can be seen as a problem in 3D, as the biological sample is imaged in 3D. CT is similar to Cryo-EM, but reconstruction is slightly simpler, since it is potentially in 2D and observation angles are known. That's why it is well suited as a first step towards a Cryo-EM algorithm.

I introduce *GAT-Denoiser*, a Graph Neural Network which combines Graph Attention Network (GAT) with convolution and an end-to-end learning approach. It enables denoising of observations and improves reconstruction quality with the assumption of known projection angles. During training, an end-to-end approach is applied, that compares reconstruction quality. GAT-Denoiser has been evaluated on the LoDoPaB-CT dataset. It could outperform baseline algorithm BM3D measured by the reconstruction signal-to-noise-ratio (SNR). An improvement by 379.9%, 126.0% 57.7%, 27.6% for SNR -15 dB, -10 dB, -5 dB and 0 dB, respectively could be reached. Moreover, the individual components of GAT-Denoiser contribute to the success of GAT-Denoiser. During a series of experiments, it was shown that convolution, GAT and end-to-end learning are all valuable individually. Further, GAT-Denoiser combined with U-Net and joint neural network training can upgrade CT reconstruction in the high-noise domain to a new level.

# Table of Contents

<b>Acknowledgments</b>	<b>ii</b>
<b>Abstract</b>	<b>iii</b>
<b>1 Introduction</b>	<b>1</b>
<b>2 Notation</b>	<b>3</b>
2.1 Molecular Imaging Methods . . . . .	3
2.2 Graphs . . . . .	3
2.3 Maths . . . . .	4
<b>3 Molecular Imaging Methods</b>	<b>5</b>
3.1 Computed Tomography . . . . .	5
3.2 Cryo-Electron Microscopy . . . . .	7
3.3 Abstraction . . . . .	8
<b>4 Manifolds and Graphs for Molecular Imaging</b>	<b>10</b>
4.1 Graph Foundations . . . . .	10
4.2 Graph Laplacian & Manifolds . . . . .	11
4.2.1 Graph Laplacian . . . . .	11
4.2.2 Graph Laplacian Embedding for Molecular Imaging . . . . .	11
4.3 Graph Denoising . . . . .	13
4.4 Graph Deep-Learning . . . . .	14
<b>5 GAT-Denoiser</b>	<b>15</b>
5.1 Pipeline . . . . .	15
5.2 Layers . . . . .	16
5.3 Training . . . . .	17
<b>6 Results</b>	<b>18</b>
6.1 Dataset . . . . .	18
6.2 Project Setup . . . . .	18
6.3 Small Scale Experiments . . . . .	19
6.3.1 Baseline . . . . .	20
6.3.2 K-NN Experiments . . . . .	20

6.3.3	GAT Experiments . . . . .	23
6.3.4	Convolution Experiments . . . . .	24
6.3.5	Loss Experiments . . . . .	25
6.3.6	GAT-Denoiser Component Experiments . . . . .	25
6.4	Large Scale Experiments . . . . .	27
6.4.1	Baseline . . . . .	27
6.4.2	GAT-Denoiser Components Experiments . . . . .	27
6.4.3	Best Models Experiments . . . . .	28
<b>7</b>	<b>Conclusion and Future Work</b>	<b>30</b>
7.1	Conclusion . . . . .	30
7.2	Future Work . . . . .	30
<b>Bibliography</b>		<b>32</b>
<b>Appendix A</b>	<b>Mathematical Tools</b>	<b>35</b>
<b>Appendix B</b>	<b>Graph Laplacian Embedding</b>	<b>37</b>
<b>Appendix C</b>	<b>Neural Networks</b>	<b>41</b>
<b>Appendix D</b>	<b>Additional Results</b>	<b>44</b>

# 1

## Introduction

**Motivation:** Inverse Problems aim to estimate an original signal that processed a system, based on potentially noisy output signal observations. They are widely used throughout different science directions, such as Machine Learning (ML), Signal Processing, Computer Vision, Natural Language Processing, and others. ML is one tool to model and solve Inverse Problems.

Cryo-Electron Microscopy (Cryo-EM) is a molecular imaging method and has received a lot of attention in recent years. During observation, the molecules are frozen and imaged through an electron microscope. Due to ground-breaking improvements regarding hardware and data processing, the field of research has been highly improved. In 2017, pioneers in the field of Cryo-EM received the Nobel Prize in Chemistry<sup>1</sup>. Today, using Cryo-EM, molecular structures can be observed with near-atomic resolution. The big challenges are enormous noise and unknown observation angles.

Computed Tomography (CT) is another imaging method, which is similar to Cryo-EM. Reconstruction is considered slightly easier as the problem is in 2D and observation angles are known. That's why it is well suited as a first step towards a Cryo-EM algorithm.

The overall goal of this Thesis is to introduce an algorithm that works with CT, but can conceptually be extended to work in 3D, thus for Cryo-EM. Additionally, the focus is in the high noise domain, as currently available reconstruction algorithms start to fail when dealing with high noise. To be more precise, the signal-to-noise-ratio (SNR) of interest is the interval between  $[-15, 0]$  dB.

In recent years, graphs have received a lot of attention in ML and Graph Machine Learning is one of the most promising research areas[12, 14, 23, 26]. Graphs are a well suited data structure, simple but with high expressiveness. Especially data for which single data points tend to have a relation to other data points, graphs with its nodes and edges are the perfect tool to capture these relationships. Real world data might be in a graph structure, like social networks, citation networks, protein interaction networks or a simple google search. If data is not available in graph structure, a graph can artificially be constructed for arbitrary datasets. Besides, for some scenarios, ordinary ML algorithms fail, but Graph ML approaches have

---

<sup>1</sup> <https://www.nobelprize.org/prizes/chemistry/2017/press-release/>

great success, e.g. dimensionality reduction for high-dimensional data.

**Contribution:** As a result of this Thesis, a Graph Neural Network (GNN) [12] architecture is proposed, which is called *GAT-Denoiser*. GAT-Denoiser aims to denoise noisy observations to improve overall reconstruction quality. The assumption of known observations angles is defined. In the GNN architecture, convolution and the Graph Attention Network (GAT) [23] are used to denoise observations. In addition, an end-to-end learning approach is used, where the reconstruction quality is compared in the loss and not only the denoised observation quality.

GAT-Denoiser was evaluated on the LoDoPaB-CT dataset [15]. I could show that all three components contribute to learning the best GAT-Denoiser model. Further, U-Net [17] was used to further improve CT reconstruction quality. GAT-Denoiser outperformed BM3D [8] as well as U-Net [17], where observation SNR is between 0 dB and -15 dB. Compared to the best performing baseline BM3D, GAT-Denoiser could improve reconstruction SNR by 379.9% for observation SNR -15 dB. The best GAT-Denoiser models could be established, when first, GAT-Denoiser is trained with a fixed U-Net model. After some learning, in a second step, GAT-Denoiser and U-Net have been trained jointly.

**Outline:** The report is structured as follows:

First, the notation applied throughout this Thesis is introduced in Chapter 2. Chapter 3 presents the two molecular imaging methods CT and Cryo-EM and mathematical abstractions for observation and reconstruction are introduced. Further, Chapter 4 is dedicated to manifolds and graphs, and how a meaningful embedding for CT and Cryo-EM can be established. The main contribution is presented in Chapter 5, where GAT-Denoiser is introduced. Chapter 6 presents experiments on the LoDoPaB-CT dataset. During small scale and large scale experiments, insights are revealed. Finally, the conclusion and future work are presented in Chapter 7.

# 2

## Notation

In this chapter, some basic terms are explained and their notation in this report is defined.

### 2.1 Molecular Imaging Methods

Throughout this Thesis, notation  $p$  for noiseless observation and  $y$  for observation with noise is used. In practice,  $p$  is not observable directly and observed signal  $y$  needs to be denoised. Further,  $x$  is used for the biological sample and  $x'$  defines approximation by the reconstruction algorithm. In addition,  $N$  is used for the number of observations and  $M$  as the observation dimension. Consequently,  $y_i \in \mathbb{R}^M$  determines  $i$ -th observation and  $y_i[j] \in \mathbb{R}$  the  $j$ -th element of  $y_i$ , with  $1 \leq i \leq N$  and  $1 \leq j \leq M$ . The same is valid for  $p$  with  $p_i$  and  $p_i[j]$ .

**Signal-to-Noise-Ratio** SNR is a measure used in Signal Processing. It compares the power of an input signal to the power of the undesired noise. It is typically given in decibel (dB), with  $\text{SNR}_{dB} = 10 \log_{10} \left( \frac{P_{signal}}{P_{noise}} \right)$ . An SNR of smaller than 0 dB indicates more noise than signal.

From a given clean image and its noisy version, SNR can be determined. During this Thesis, the term SNR is used in two scenarios. First, to indicate how much noise is present in  $y$ . Second, as a quality measure for reconstruction. To make notation clear,  $SNR_y$  is used to express the level of noise in  $y$ , where SNR is computed from  $y$  and  $p$ . Contrary,  $SNR$  refers to SNR computed from  $x'$  and  $x$ .

### 2.2 Graphs

A graph is defined as  $G = \langle V, E \rangle$ , where  $V$  is a set of vertices (or nodes) and  $E$  is a set of edges (or links). Edges are defined as a set of tuples  $(i, j)$ , where  $i$  and  $j$  determine the index of vertices in the graph.

**Graph Properties:** A graph can be either *directed* or *undirected*. In a directed graph, an edge connects explicitly from one node to another, consequently edge  $(i, j) \neq (j, i)$ .

In an undirected graph, edges have no direction, and ordering does not matter, therefore  $(i, j) = (j, i)$ . Throughout this Thesis, undirected graphs are considered, and when writing from a graph, is refers to an undirected graph.

The *neighborhood*, denoted by  $\mathcal{N}(i)$ , of a node  $i$  is defined as all adjacent nodes. In other words, there is an edge between neighborhood nodes and  $i$ . Further, edges can have *weights*, which is a method to distinguish between the importance of neighbors, resulting in a *weighted* graph. *Degree* of a node is the number of incoming edges.

**Adjacency Matrix:** The (binary) adjacency matrix of graph  $G = \langle V, E \rangle$  is defined as follows:

$$A_{ij} = \begin{cases} 1 & \text{if } (i, j) \in E \\ 0, & \text{otherwise} \end{cases} \quad (2.1)$$

Matrix  $A$  has dimension  $\mathbb{R}^{N \times N}$  with  $N$  as number of nodes and indices of  $A$  correspond to nodes in  $V$ . If there exists an edge between two nodes, entry in  $A$  will be set to 1, otherwise to 0. This leads to an unweighted graph, as the weights of all edges will be 1. When  $G$  is undirected, the corresponding adjacency matrix will be symmetric. Eigenvalues of  $A$  are called *spectrum* of  $G$ .

**Graph Construction with k-NN:** K-Nearest-Neighbors (k-NN) is a graph construction algorithm. The affinity between nodes is calculated with a distance measure (e.g. Euclidean distance) and for every node,  $\mathcal{N}_i$  is defined as  $k$  nodes with the smallest similarity measure. During this Thesis, when writing from  $k$ , it refers to the k-NN parameter  $k$ .

**Erdős–Rényi graph** The Erdős–Rényi model is a way to construct a random graph. For a set of nodes, a graph is constructed by connecting nodes randomly. Every possible edge has the same probability to be present in the graph, which is determined by parameter  $p$ .

## 2.3 Maths

**Convolution:** During this Thesis, symbol  $\star$  is used for the convolution operator.

**Concatenation:**  $\parallel$  is used for the concatenation operator, which combines vectors end-to-end. For vectors  $x = (x_0, \dots, x_n)$  and  $y = (y_0, \dots, y_n)$  concatenation is defined as  $x \parallel y = z$  with  $z = (x_0, \dots, x_n, y_0, \dots, y_n)$ . The operator can be applied to an arbitrary number of vectors. Consider  $N$  vectors  $v_1, \dots, v_n$ , concatenation is written as  $\parallel_{i=1}^N v_i$ .

# 3

## Molecular Imaging Methods

This chapter introduces two molecular imaging methods, *Computed Tomography* (CT) and *Cryo-Electron Microscopy* (Cryo-EM). Their observation model is defined in a mathematical way and reconstruction is presented. Finally, an abstraction is presented, as both methods are considered similar.

### 3.1 Computed Tomography

CT is a well established molecular imaging method. Using X-ray sources, fan shaped beams are produced which scan the biological sample. Through scanning over straight lines, many observations are collected, and the biological sample can be reconstructed<sup>2</sup>.

**2D Tomographic Observation:** Mathematically, CT observations are defined as follows:

$$\begin{aligned} y_i[j] &= p_i + \eta_i[j] && \text{with } 1 \leq i \leq N \text{ and } 1 \leq j \leq M \\ &= R(x, \theta_i, s_j) + \eta_i[j] && \text{with } 1 \leq i \leq N \text{ and } 1 \leq j \leq M \end{aligned} \tag{3.1}$$

with

- $x \in L^2(\Omega)$  : biological sample with  $\Omega \subset \mathbb{R}^2$  and  $L^2$  Lebesgue space
- $R(\cdot; \theta_i, s_j) : L^2(\Omega) \rightarrow \mathbb{R}^M, x \mapsto R(x; \theta_i, s_j)$  : Radon Transform<sup>3</sup> with  $\theta_i \in SO(2)$  as observation angle and  $s_j \in \mathbb{R}$  as sampling point
- $\eta_i \in \mathbb{R}^M$  : i.i.d Gaussian noise with  $\eta_i[j] \sim \mathcal{N}(0, \sigma^2) \in \mathbb{R}$

**Observation Illustration:** The output of Radon Transform is called a *sinogram*, which is a synonym for the CT observation. In Figure 3.1(a) the Shepp-Logan phantom is illustrated. It is often used as an image for simulating a brain CT, and it refers to the biological sample  $x$ . Further, in Figure 3.1(b) and Figure 3.1(c) sinograms are presented with and without noise

<sup>2</sup> For additional information [2]

<sup>3</sup> For additional information [21]

respectively. For this example,  $\theta \in \mathbb{R}^{500}$  was evenly spaced between  $[0, 2\pi]$  and  $\text{dim}(s) = 400$ . Thus,  $p \in \mathbb{R}^{500 \times 400}$  and noise is added to reach an  $\text{SNR}_y$  of 10 dB.

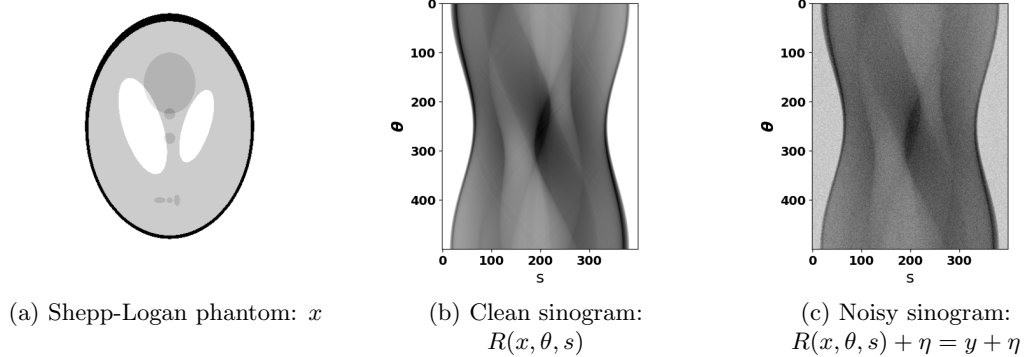


Figure 3.1: Shepp-Logan phantom and sinograms.

**Tomography Reconstruction:** CT reconstruction is a popular Inverse Problem. The aim is to reconstruct a biological sample based on observations. When the biological sample is in 2D, observations are available in 1D. The reconstruction is possible for 3D objects too, where observations are in 2D. In this Thesis, I will focus on the 2D case of CT.

**Filter Backprojection:** Filter Backprojection (FBP) [5] is a reconstruction method used in CT. Until recently, it was the primary method for reconstruction as it allows to inverse the Radon Transform, resulting in  $x'$  which  $\approx x$  for the noiseless case.

FBP can be defined as:

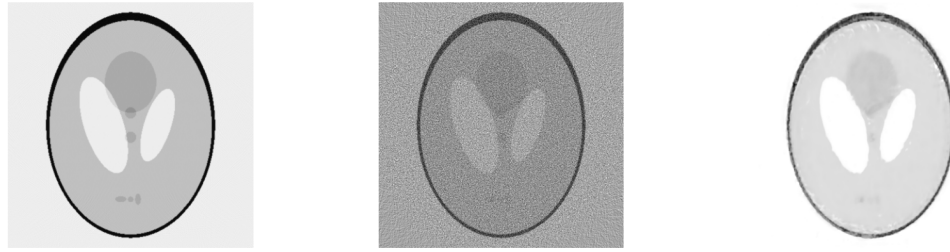
$$\text{FBP}(\cdot; \theta, s) : \mathbb{R}^{M \times N} \rightarrow \mathbb{R}^{M \times M}, y \mapsto \text{FBP}(y; \theta, s) = x' \quad (3.2)$$

Where  $\theta$  are projection angles and  $s$  are the sampling points. But, the algorithm fails when working with highly noisy data [18], as it is not possible to draw meaningful connections any longer, noise is dominating information in the data.

Therefore, alternatives for the high noise domain have been studied in recent year. Lately, neural network approaches emerged, which further processed the output of FBP to increase reconstruction quality. This is the approach I will follow in this Thesis. Leuschner et al. [16] compared different Deep-Learning reconstruction methods for CT.

**U-Net:** Today's state-of-the-art reconstruction algorithms are Deep-Learning based. U-Net [17], a convolution neural network, performed much better compared to FBP in the comparison of Leuschner et al. [16]. Therefore, it is an interesting baseline and additionally can be combined with other ideas.

In Figure 3.2 reconstructions from Shepp-Logan phantom are presented.  $\text{SNR}_y$  is defined to reach 10 dB. The quality of the noisy reconstruction is rather low, some important details are missing, and noise dominates reconstruction. If more noise is present in  $y$ , the reconstruction will be of even lower quality. Further, Figure 3.2(c) shows reconstruction with U-Net where some details are missing as well, although overall noise is drastically decreased.



(a) Clean reconstruction:  
 $FBP(p, \theta, s)$

(b) Noisy reconstruction:  
 $FBP(y, \theta, s)$

(c) Noisy reconstruction:  
 $UNet(FBP(y, \theta, s))$

Figure 3.2: Shepp-Logan reconstructions with  $\text{SNR}_y$  10 dB.

### 3.2 Cryo-Electron Microscopy

Cryo-EM is another molecular imaging method, that enables the view of molecules in near-atomic resolution. In this Thesis, for simplicity, only single-particle Cryo-EM [9] is considered. When writing about Cryo-EM it always refers to single-particle Cryo-EM.

During imaging, molecules are frozen in a thin layer of ice, where they are randomly oriented and positioned. Random orientation and positioning make reconstruction challenging, but freezing allows observation in a stable state where molecules are not moving. 2D tomographic projections of molecules are observed with an electron microscope, which are called *micrograph*. Frozen molecules are fragile, and the electron microscope needs to work with very low power (electron dose), resulting in highly noisy observations. The resulting SNR is typically smaller than 0 dB [18].

In addition, observed molecules are not equal in the sense that there are some structural varieties between molecules (isotopes). While observing the same molecule in ice many times, single observations could be from different isotopes.

**3D Cryo-EM observation:** Mathematically, observation is defined as follows:

$$\begin{aligned} y_i &= p_i + \eta_i && \text{with } 1 \leq i \leq N, \\ y_i &= \Pi_z(\text{Rot}(x; \theta_i)) + \eta_i && \text{with } 1 \leq i \leq N, \end{aligned} \tag{3.3}$$

where

- $x \in L^2(\Omega)$ : biological sample with  $\Omega \subset \mathbb{R}^3$
- $\Pi_z : L^2(\Omega) \rightarrow L^2(\tilde{\Omega})$ ,  $x \mapsto \int x(\cdot, \cdot, z) dz$ : z-axis projection operator with  $\tilde{\Omega} \subset \mathbb{R}^2$
- $\theta_i = [\theta_i^{(1)}, \theta_i^{(2)}, \theta_i^{(3)}]$ : 3D rotation matrix with  $\theta_i^{(1)}, \theta_i^{(2)}, \theta_i^{(3)} \in [0, 2\pi]$  and  
 $R_{\theta_i} = R_{e_x}(\theta_i^{(1)})R_{e_y}(\theta_i^{(2)})R_{e_z}(\theta_i^{(3)}) = [R_{\theta_i}^1, R_{\theta_i}^2, R_{\theta_i}^3] \in SO(3)$ <sup>4</sup>
- $\text{Rot} : L^2(\Omega) \rightarrow L^2(\Omega)$ ,  $\text{Rot}(x, \theta_i) = ((x_1, x_2, x_3) \mapsto (x_1 R_{\theta_i}^1, x_2 R_{\theta_i}^2, x_3 R_{\theta_i}^3))$ : rotation operator

<sup>4</sup> For additional information see A.1

- $\eta_i \in \mathbb{R}^M$ : i.i.d Gaussian noise with  $\eta_i[j] \sim \mathcal{N}(0, \sigma^2) \in \mathbb{R}$

Equation 3.3 is a simplified version of Cryo-EM. First, the point spread function of the microscope is not taken into account. Second, structural variety is ignored, the underlying sample  $x$  is not the same for every observation. Precisely,  $x$  can be seen as a random signal from an unknown distribution defined over all possible molecule structures. In this Thesis, only the simplified version is considered.

Moreover, as  $y_i$  is not observable directly, discretization is needed:

$$\begin{aligned} y_i &= (\Pi_z(\text{Rot}(x; \theta_i)) + \eta_i)(\Delta) && \text{with } 1 \leq i \leq N \\ y_i[j, k] &= \Pi_z(\text{Rot}(x; \theta_i))_{j, k} + \eta_i[j, k] && \text{with } 1 \leq i \leq N \text{ and } 1 \leq j, k \leq \sqrt{M} \end{aligned} \quad (3.4)$$

With

- $\Delta \in \tilde{\Omega}^M$ : sampling grid with dimension  $M$
- $y_i[j, k]$ ,  $\eta_i[j, k]$  and  $\Pi_z(\cdot)_{j, k} \in \mathbb{R}$  with  $j, k$  as indices of the sampling grid.

**Observation Illustration:** In Figure 3.3 Cryo-EM micrographs are illustrated as well as the reconstructed biological sample.

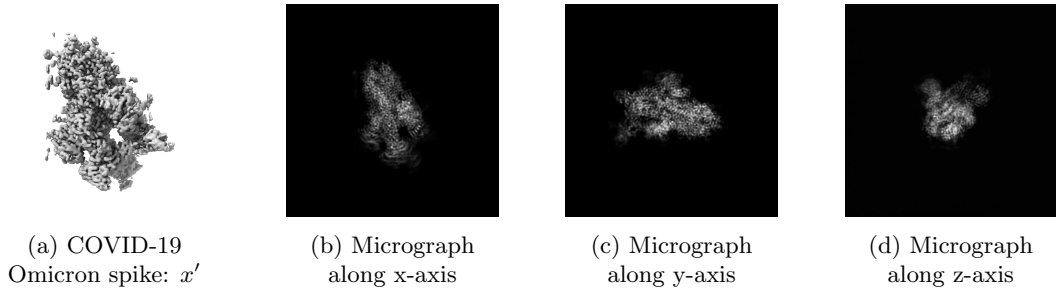


Figure 3.3: Cryo-EM reconstruction and micrographs of COVID-19 Omicron spike<sup>5</sup>.

**Cryo-EM Reconstruction:** Cryo-EM reconstruction is defined as the approximation of a 3D object from 2D observations. Cryo-EM reconstruction is computationally intensive and multiple steps are required to get from observations to the final structure<sup>6</sup>.

### 3.3 Abstraction

As CT and Cryo-EM are highly related, the aim of this section is to define an abstraction model. The big difference is, that CT is in 2D and Cryo-EM in 3D. Mathematically, an extension from 2D to 3D should be theoretically feasible. It is considered a numerical challenge due to the need of additional computing resources. Therefore, an abstract form will be defined. A similar notation than previously is used, with the biological sample  $x \in L^2(\Omega)$ . Further, the biological sample dimension space is parametrized with  $D$ , consequently  $\Omega \subset \mathbb{R}^D$ . Additionally, dimension of observation space is defined as  $D - 1$ , such that  $\tilde{\Omega} \subset \mathbb{R}^{D-1}$ .

<sup>5</sup> <https://www.ebi.ac.uk/emdb/EMD-32500>

<sup>6</sup> For additional information [1, 9]

$$\begin{aligned} y_i &= p_i + \eta_i(\Delta) && \text{with } 1 \leq i \leq N \\ y_i &= (A(x, \theta_i) + \eta_i)(\Delta) && \text{with } 1 \leq i \leq N \end{aligned} \quad (3.5)$$

with

- $x \in L^2(\Omega)$ : biological sample
- $A : L^2(\Omega) \rightarrow \mathbb{R}^M, x \mapsto A(x; \theta_i)$ : a non-linear operator
- $\theta_i \in SO(D)$ : projection angle(s) vector, with  $P$  projection dimension
- $\eta_i \in \mathbb{R}^M$ : i.i.d Gaussian noise with  $\eta_i[j] \sim \mathcal{N}(0, \sigma^2) \in \mathbb{R}$
- $\Delta \in \tilde{\Omega}^M$ : term for discretization

**Reconstruction:** Further, an abstract form of the reconstruction operator is defined as:

$$Recon : \mathbb{R}^{M \times N} \rightarrow \mathbb{R}^{M \times M}, y \mapsto Recon(y; \theta) \quad (3.6)$$

With  $\theta_i \in SO(D)$  as the projection angle(s).

For CT, parameter  $D = 2$  and  $A(\cdot)$  is the Radon Transform. Further, reconstruction operator can be defined as FBP (with or without U-Net). Cryo-EM parameters are defined with  $D = 3$  and  $A(\cdot)$  can be defined as  $\Pi_z(\text{Rot}(x; \theta))$ .

**High Noise Regime:** Cryo-EM observations are highly noisy, which makes reconstruction challenging. There are different ways to reduce noise from observations, most of them are related to averaging. Averaging needs to consider similar observations and ignore diverse ones. In the defined abstract model, averaging over paired observations from  $\theta$  should be a good averaging model.

One idea would be to measure distances between observations. Another way is to find a low-dimensional embedding which maps observation  $y$  to  $\theta$ . When talking from low-dimensional embeddings, there is no way around Graph Laplacian and Graph Learning, which will be introduced in the next chapter.

# 4

## Manifolds and Graphs for Molecular Imaging

In this chapter, the connection between graphs and Graph Laplacian (GL) embedding to CT and Cryo-EM is examined. First, an introduction to Graph Learning is presented, and it is shown how a graph for CT and Cryo-EM observations can be constructed. Second, GL and its embedding are introduced and the connection to CT and Cryo-EM is illustrated. Further, the term Graph Denoising is introduced and last, some Graph Deep-Learning approaches are presented.

### 4.1 Graph Foundations

**Graph Learning:** Graph Learning has received a lot of attention in recent years. The idea is to learn graph information, such as topology or connections between nodes, to solve tasks. Attention mechanisms are popular at the moment [22] and the idea was derived to graphs [23]. It resumes to computing node features by using local information, therefore, the neighborhood of nodes is exploited. Popular learning tasks are *node classification* or *link prediction*. A model is learned from node and edge features as well as topology, hopefully enabling adequate node classification or prediction of a link. Another common task is *community detection*, which aims to identify clusters of nodes within the input graph. Further, graphs are highly favored for *dimensionality-reduction*, where graph algorithms provide a helpful tool, while ordinary algorithms like principal component analysis fail to establish a meaningful dimensionality reduction.

**Constructing Graphs for Molecular Imaging:** For a Cryo-EM or CT observation, a graph can be constructed. Every observation  $y_i$  can be assigned to a node  $v_i$ , consequently  $v_i \in \mathbb{R}^M$  and  $|V| = N$ .

To determine affinity between two nodes, a distance measure needs to be defined. For CT, it can be set up by using the  $\ell_2$ -norm  $\|y_i - y_j\|_2^2$ . A Cryo-EM distance measure is more challenging to set up, as observations include a random 3D rotation and a 2D projection. Two observations might be equivalent up to a 2D rotation. Consider a first observation  $y_1$ , which has no 3D rotation and a second observation  $y_2$  with a rotation in x-y plane by  $45^\circ$ . The two projections have a defined in-plane rotation  $g$ , such that  $g y_1 = y_2$ . Therefore, a

term of in-plane rotation is added to the  $\ell_2$ -norm:  $\min_{g \in SO(2)} \|g y_i - y_j\|_2^2$ , which is inspired by [10].

## 4.2 Graph Laplacian & Manifolds

In the following section, the connection of GL and manifolds to CT and Cryo-EM is established.

### 4.2.1 Graph Laplacian

GL is a matrix that represents a graph and can be used to find many important properties. It is a very powerful tool and a good introduction can be found in [20, 24].

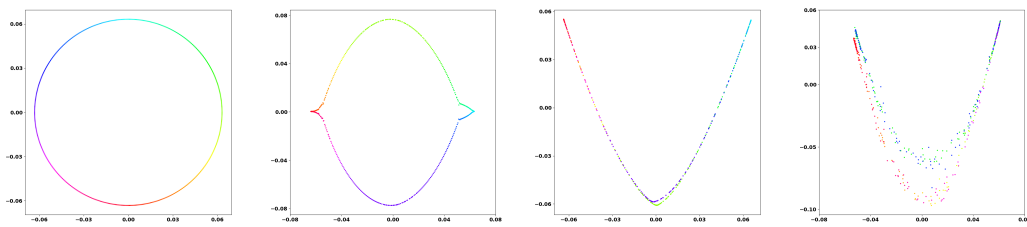
GL is defined as  $L = D - A$ , with  $A$  as the adjacency matrix and  $D$  the degree matrix (diagonal matrix with the degree of nodes as entries).

### 4.2.2 Graph Laplacian Embedding for Molecular Imaging

A basic introduction to GL embedding and how it can be computed is found in Appendix B.1. In this section, the connection to CT and Cryo-EM is established directly.

For a given observation, a low-dimensional embedding can be computed by using the GL. To be more precise, the second and third smallest eigenvectors of GL are computed and will be observed in an example with the Shepp-Logan phantom. For the Radon Transform,  $\theta$  and  $s$  are specified with  $\theta \in \mathbb{R}^{500}$  as evenly spaced between  $[0, 2\pi]$  and  $\dim(s) = 200$ .

In Figure 4.1(a), the embedding calculated from clean sinogram and  $k = 2$  is illustrated. It looks like a perfect circle and the angles are in order. Further, noise was added to the sinogram to reach  $\text{SNR}_y$  20 dB, 10 dB and 0 dB. Additionally, the embedding was computed with  $k = 6$  and illustrated in Figure 4.1(b), Figure 4.1(c) and Figure 4.1(d) respectively. For  $\text{SNR}_y$  20 dB a circle-like shape could be established, for  $\text{SNR}_y$  10 dB it looks like a half circle and for  $\text{SNR}_y$  everything is scattered.



(a) Clean sinogram GL embedding  $k = 2$    (b) GL embedding  $k = 6$  with  $\text{SNR}_y$  20 dB   (c) GL embedding  $k = 6$  with  $\text{SNR}_y$  10 dB   (d) GL embedding  $k = 6$  with  $\text{SNR}_y$  0 dB

Figure 4.1: GL embeddings from Shepp-Logan phantom sinograms.

In the fields of CT and Cryo-EM, the underlying low-dimensional manifold is well-defined for noiseless data and was observed with the GL embedding. The manifold in 2D is a circle, whereas in 3D it is defined as a sphere. This fact can be exploited during learning.

**Tomography for unknown Angles:** But what can we use this embedding for? It is defining a low-dimensional mapping from high-dimensional space. Coifman et al. [7] derived that, in the case of CT, this embedding approximates the angles of observations. Therefore, for (noisy) observations, angles are approximated and reconstruction can be computed even if angles are unknown. The challenge is the quality of the embedding. As long as the computed embedding is a mapping to the circle (or sphere), it should be reasonable to do reconstruction with. In Figure 4.2 reconstruction with unknown angles is illustrated. Again,  $k = 6$  and  $\text{SNR}_y$  20 dB and 0 dB are applied. Clean reconstruction with approximated angles in Figure 4.2(a) looks good, despite, that there is an in-plane rotation of around 45 degrees. But even for moderate noise of  $\text{SNR} 20 \text{ dB}$ , where the embedding looks circle-like (Figure 4.1(b)), the difference between reconstruction with known angles (Figure 4.2(d)) and unknown angles (Figure 4.2(b)) is massive. For 0 dB, already with known angles (Figure 4.2(e)), reconstruction fails and with unknown angles barely anything from the original Shepp-Logan phantom can be determined (Figure 4.2(c)).

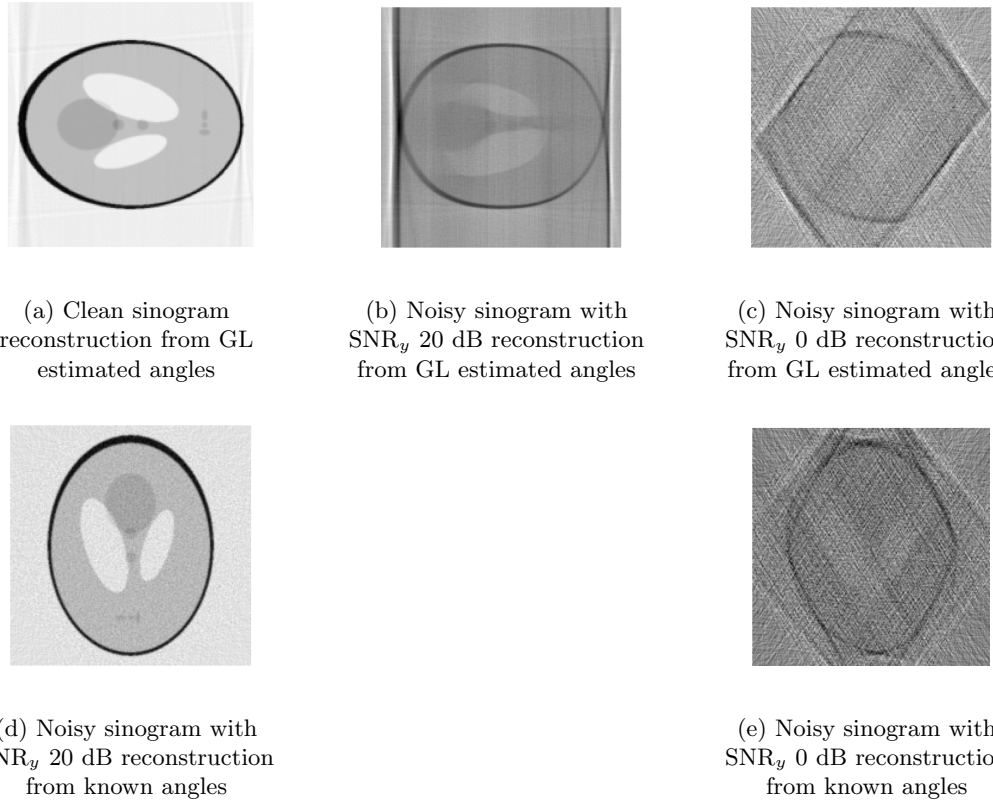


Figure 4.2: Shepp-Logan phantom reconstruction with approximated angles.

Not only noise is reducing the GL embedding quality, but  $k$ , number of observations and observation dimension have an impact on the final result. Their importance to the GL embedding is presented in Appendix B.1.1.

With the GL embedding, observation angles can be approximated. Therefore, CT and Cryo-EM problem can be solved for unknown angles with moderate noise.

**Observation Denoising:** As the quality of reconstruction is highly dependent on observations, it is expected to increase when the level of noise is decreased. Therefore, standard denoising methods like Block-matching and 3D filtering (BM3D) [8] or non-local means [3] could be applied to denoise observations to get higher quality reconstructions. Both algorithms emerged from Signal Processing and are not operating on a graph structure. But, they use a neighborhood for averaging, which shows great potential for graph as a data structure for denoising, as graphs can represent neighborhoods really well. BM3D is considered the state-of-the-art denoising algorithm, before algorithms emerged from Deep-Learning. Therefore, it will be applied as a baseline algorithm in the practical part. Further, as illustrated with the GL embedding, graphs can restore information with a suitable prior, such as angles are uniformly sampled on the unit-circle (unit-sphere).

### 4.3 Graph Denoising

*Graph Denoising* is not a common term in literature. A way of constructing a k-NN graph from observations was introduced. Our constructed graph from observations can be considered a noisy graph, as observations are noisy. Moreover, the underlying low-dimensional manifold was analyzed with the GL embedding, which is a circle or a sphere. This entails, that in the noiseless case, the GL embedding maps data points to the circle (sphere), where a graph can be easily constructed, neighboring nodes on the circle can be connected. As a consequence, it can be considered to be known how the noiseless graph looks like in the low-dimensional space, but not for original high-dimensional space. The goal of Graph Denoising is to estimate the original graph  $G$  from a given noisy graph  $G_0$ . In other words, noisy graph  $G_0$  will be denoised. This is my definition for Graph Denoising, which is rather related to signal or image denoising. For every noisy graph there exists an original graph  $G = \langle V, E \rangle$ . The noisy graph  $G_0$  can further be defined as  $G_0 = \langle V, E_0 \rangle$ , where  $E_0 = E \setminus E_0^- \cup E_0^+$  with  $E_0^- \subseteq E$  and  $E_0^+ \cap E = \emptyset$ .

$G_0$  consists of the same nodes  $V$  as  $G$ . From  $E$  some edges are removed (denoted by  $E_0^-$ ) and some are added (denoted by  $E_0^+$ ).

**Connection to Link Prediction:** Link Prediction is a common task in Graph Learning. The goal is to predict the existence of a link between two nodes. The task can be formulated as a missing value estimation task. A model  $M_p$  is learned from a given set of observed edges. The model finally maps links to probabilities  $M_p : E' \rightarrow [0, 1]$  where  $E'$  is the set of potential links.

Further,  $U$  determines the set of all possible links of  $G$ , therefore  $E \subseteq U$ . Clearly, Graph Denoising can be seen as a Link Prediction problem. The difference is, that in Link Prediction a model from a set of observed links is learned  $E' \subseteq E$  and in Graph Denoising model is learned from  $E' \subseteq U$ . Link Prediction problems are a subset of Graph Denoising problems.

#### 4.4 Graph Deep-Learning

The state-of-the-art methods for solving Link Prediction are *Graph Deep-Learning* approaches. With GNN [12] the framework for neural networks with graphs has been established.

Using Graph Convolutional Networks (GCN) [14] for graph feature extraction is a popular way. With GCN a new feature representation is iteratively learned for node features (edge features are not considered). It can be seen as an averaging of nodes over their neighborhood where all neighbors get the same weight combined with some non-linear activation (e.g. Rectified Linear Unit). To consider the node itself in averaging, Kipf and Welling [14] applies the so-called "Renormalization trick", where self-loops are added to the adjacency matrix and after every layer, a normalization step is applied. The topology of the graph will not be adjusted during the learning process.

Simple Graph Convolutional Network [26] proposed a simplified version of GCN. They could verify their hypothesis that GCN is dominated by the local averaging step and non-linear activation function between layers does not contribute too much to the success of GCN. Therefore, it can be seen as a way of power iteration<sup>7</sup> over the adjacency matrix with normalization in every layer. Wang et al. [25] proposed an extension to GCN by not operating on the same graph in every layer but adopting underlying graph topology layer by layer. GAT [23] extends the concept of GCN with attention where not all neighboring nodes get the same weight (attention). Again, the topology of the graph will not change, but weighted averaging over the neighborhood will be computed and this is what in denoising is a good idea.

---

<sup>7</sup> For additional information A.2

# 5

## GAT-Denoiser

In this chapter, I will introduce my methodological approach. As a result, a GNN is derived which is called *GAT-Denoiser*. Its main components and overall architecture are introduced. GAT-Denoiser is implemented for 2D CT and therefore, some details for the 2D case are presented.

**Goal:** CT and Cryo-EM in the high-noise regime is the domain of interest. For a given set of observations, a denoising model is sought, while it enables denoising of observations such that reconstruction quality increases. As a first step toward an algorithm that works for unknown observation angles, angles are fixed during the practical part of this Thesis.

**Input Graph:** As  $\theta$  is fixed, angles corresponding to each observation are known. Therefore, a graph can be constructed to model neighboring observations based on their angles. To define a distance measure, angles can be mapped to the unit circle (or sphere). Then, a geodesic distance can be computed with the great-circle distance. Based on these distances, a k-NN graph can be constructed.

For GAT-Denoiser, fixed angles entails that graph topology is fixed and a k-NN graph can be constructed from  $\theta$ .

### 5.1 Pipeline

The GAT-Denoiser pipeline consists of three neural network parts, namely convolution, GAT and U-Net. Appendix C presents an introduction for readers who are not familiar with these concepts.

GAT-Denoiser is a GNN and has two main components, namely convolution layers and GAT layers. The main idea of GAT-Denoiser is to enable denoising of observations:

$$GAT\text{-}Denoiser(\cdot) : \mathbb{R}^{N \times M} \rightarrow \mathbb{R}^{N \times M}, y \mapsto GAT\text{-}Denoiser(y) \quad (5.1)$$

Input  $y$  of GAT-Denoiser is a noisy observation and the output is a denoised version. GAT averages over observation neighbors and convolution denoise single observations. For every

GAT layer there is a preceding convolution. In the case of CT, convolution is in 1D, where for Cryo-EM it is in 2D.

The GAT denoise the observation signal with its neighbors by averaging. Further, convolution is added to denoise single observations.

In Figure 5.1 the GAT-Denoiser pipeline is illustrated. The main overall goal is to get the best possible  $x'$  from  $y$  and not just denoise  $y$  to approximate  $p$ .

$$x \approx \text{Recon}(\text{GAT-Denoiser}(y)) = x' \quad (5.2)$$

Therefore, an end-to-end learning approach is used where quality of reconstruction is compared during GAT-Denoiser training, which is expected to perform better than only optimizing denoising of observations.

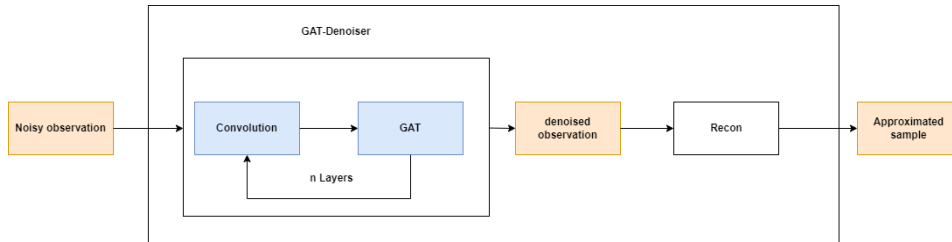


Figure 5.1: GAT-Denoiser pipeline.

## 5.2 Layers

The input to the neural network layers are observations and output are denoised observations. Thus, input and output dimension is defined as  $\mathbb{R}^{N \times M}$ .

Figure 5.2 presents the detailed GNN architecture. It is parametrized with *channels*, *heads* and *layers*. The number of channels in convolution can be increased with parameter *channels*. Further, *heads* determines the number of heads used in the GAT layers and parameter *layers* defines how many convolution and GAT layers are stacked together in the network.

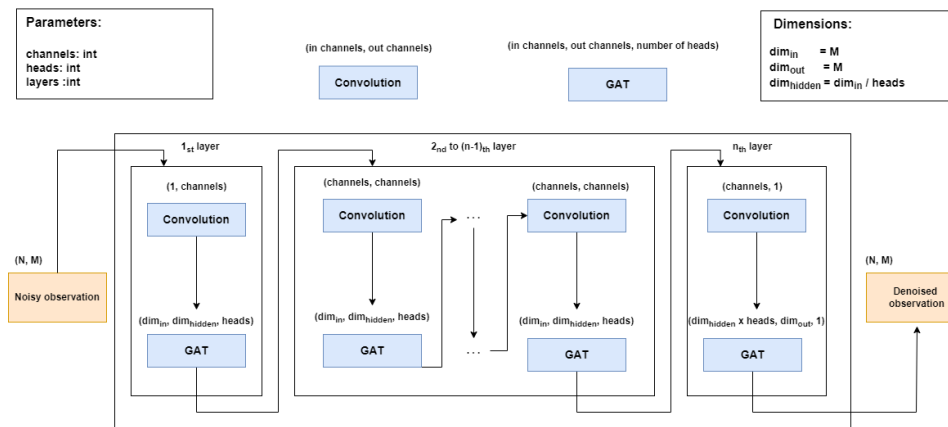


Figure 5.2: GAT-Denoiser layers.

For every layer, first convolution and then GAT is processed. As the input and output dimension is the same for GAT, convolution needs to be defined, such that the size of the input signal is the same as the size of the output signal (e.g. kernel size 3 and padding 1). Further, additional convolutional channels might be applied for learning. If parameter  $channels > 1$ , channels are increased in the first convolution layer and decreased in the last one. Parameter  $heads$  controls the multi-head approach of GAT. The input and hidden dimension of GAT is  $M$ , when no heads are applied. If multi-head attention is applied, hidden dimension will be set to  $\frac{M}{heads}$ . In the last GAT layer, everything gets prepared for output dimension and averaging with 1 head is applied.

**K-hop Neighborhood:** In GNNs, multiple layers expose the k-hop neighborhood. Thus, for a network with  $k$  layers, the network operates in the  $k$ -hop neighborhood. In GAT-Denoiser, this corresponds to the layers of GAT.

### 5.3 Training

For GAT-Denoiser, one could think of two different losses to use during training. First, the loss could be defined on an observation level, denoted by  $\mathcal{L}_{sino}$ . The  $\ell_2$ -norm is giving a meaningful measure:

$$\mathcal{L}_{sino} = \| p - \text{GAT-Denoiser}(A(x, \theta, s) + \eta) \|_2^2 \quad (5.3)$$

Second idea is to use an end-to-end learning approach where quality of reconstruction is compared in the loss. Thus, the output of GAT-Denoiser is not directly part of the loss, but first reconstruction will be computed. As the quality of the reconstruction is measured in the loss, resulting model is expected to be optimized for reconstruction quality, and not observation quality. But, it is expected to be more computing expensive, as reconstruction is needed to be calculated during training.

$$\mathcal{L} = \| x - \text{Recon}(\text{GAT-Denoiser}(A(x, \theta, s) + \eta)) \|_2^2 \quad (5.4)$$

Access to biological sample  $x$  or clean observation  $p$  is required during training, depending on the applied loss.

**Dropout:** Dropout is used in neural networks for regularization, thus to prevent over fitting. During training the neural network, some units are randomly omitted. Therefore, the network is considered to not over fit to single units, as during learning they are not always present. There is a dropout parameter in GAT, which can be considered during training.

**Reconstruction for Computed Tomography:** Reconstruction in CT is defined with U-Net, as  $\text{Recon} : \text{UNet}(\text{FBP}(\cdot))$ . Thus, U-Net needs to be first pre-trained with the desired dataset. Then, in a second step, one could consider to jointly train U-Net with GAT-Denoiser.

# 6

## Results

In this chapter, the results of GAT-Denoiser evaluation are presented. First, the LoDoPaB-CT dataset is introduced. Second, the project setup and shared settings during evaluation are defined. Third, small scale GAT-Denoiser experiments are presented, where the goal is to find good parameters for training the GAT-Denoiser model. Last, the large scale GAT-Denoiser experiments are presented, where the goal is to find the best model.

### 6.1 Dataset

GAT-Denoiser is tested on the LoDoPaB-CT [15] dataset, which is a benchmark dataset for low-dose CT reconstruction methods and, therefore, well suited for our domain.

The dataset consists of 35'820 train samples and 3'553 test samples. All of them are having resolution 64x64.

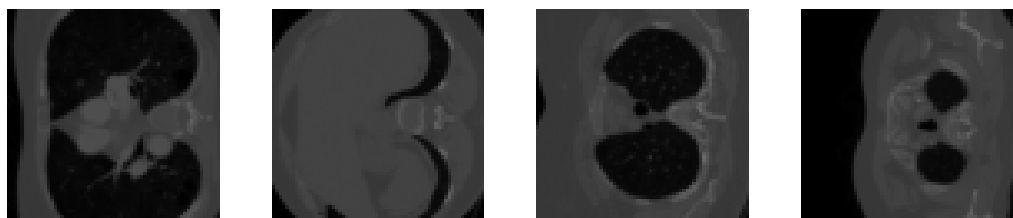


Figure 6.1: Some samples from the LoDoPaB-CT dataset.

### 6.2 Project Setup

The python source code of the project is available on GitHub<sup>8</sup>. Several python packages are used and the most important one are: Pytorch geometric<sup>9</sup> for neural network configuration, Operator Discretization Library<sup>10</sup> for Radon Transform and FBP, and last, Weight & Bias<sup>11</sup> (wandb) to gather results in a convenient way.

<sup>8</sup> <https://github.com/cedricmendelin/master-thesis>

<sup>9</sup> <https://pytorch-geometric.readthedocs.io/en/latest/>

<sup>10</sup> <https://odlgroup.github.io/odl/>

<sup>11</sup> <https://wandb.ai/site>

Training of GAT-Denoiser has been performed on the HPC-cluster scicore of the University of Basel. During training, up to 4 titanx GPUs with each 12 GB RAM have been used.

**Radon Transform:** For Radon Transform, sampling points have been fixed to 64, thus  $s \in \mathbb{R}^{64}$ . Further, projection angles  $\theta$  are sampled within interval  $[0, \pi]$ . The number of observations is the size of our input graph nodes, where typically 1024 are used.

**GAT Settings:** In the GAT layers exponential linear unit (ELU) was applied as an activation function. Further, dropout is used as a regularization term. During training, Adam [13] optimizer was applied with learning rate 0.01 and weight decay 0.0005. Moreover, mini batch gradient descent with a batch size of 64 was applied during training.

**Performance Metrics:** During evaluation, two main metrics are considered. First, *Loss* is taken into account, which refers to the average  $\ell$ -2 distance between the biological sample and reconstruction. Second, *SNR* is used, which refers to SNR in dB of reconstruction, compared to the biological sample. Further, visual results are presented and can be seen as a third metric.

**U-Net Training:** U-Net was pre-trained on the LoDoPaB-CT training dataset, with 128 channels in the first contracting step. In total, 4 steps have been computed, which results in 1024 channels as output of last contracting step. During training, noise was sampled from normal distribution to reach SNR in the interval  $[0, -10]$  dB and was added to the observation. In total, the model was trained for 200 epochs on the complete LoDoPaB-CT dataset.

**BM3D:** In the GAT-Denoiser pipeline, first, observations will be denoised, and second, reconstruction is computed. Therefore, BM3D can be applied at two different steps. First, it can be used to denoise sinogram and forward denoised sinogram to FBP, which is how GAT-Denoiser works. Secondly, FBP can be computed with noisy sinogram and output can be forwarded to BM3D, which will denoise reconstruction. In the following term *BM3D-sino* and *BM3D-reco* are used to distinguish between the two approaches.

### 6.3 Small Scale Experiments

For small scale experiments, not the complete LoDoPaB-CT dataset was considered, but only 1024 train images and 100 validation images. The default settings for GAT-Denoiser have been:  $\text{SNR}_y$  -5 dB, U-Net omitted during reconstruction, convolution with one channel, kernel size 3 and padding 1. If nothing else mentioned, these settings are applied. Models have been trained for 200 epochs. Based on 100 test samples, SNR and Loss metrics have been computed as well as visual results. Wandb experiment results can be found in Appendix D.6.

In the following sections, the results of the baseline algorithms will be presented. Further, experiments with different input graphs and  $k$  are shown. Moreover, the individual

GAT-Denoiser pipeline components are tested in isolation. Experiments with different GAT parameters, convolution settings and Loss are presented step-by-step. Finally, different promising architectures have been evaluated to finalize the small scale experiment.

### 6.3.1 Baseline

Table 6.1 shows baseline results for FBP, BM3D-sino, BM3D-reco and U-Net. Noise was added to reach  $SNR_y$  of 0, -5, -10 and -15 dB.

As expected, reconstruction with FBP performs the worst, as it only reconstructs from noisy observation. BM3D-sino and BM3D-reco perform surprisingly well for higher  $SNR_y$ . However, for lower  $SNR_y$  the algorithm performs poorly. Figure 6.2 illustrates the reconstruction of a single observation for all baseline algorithms.  $SNR_y$  is set to 0 dB.

U-Net reconstruction looks visually best, even though the SNR was lower compared to the BM3D approaches. After some investigation, a small bug in the pre-trained U-Net model was found. There was an issue with the amplitude of U-Net reconstruction, therefore the SNR values of U-Net are expected to be slightly better. But also the pre-trained U-Net model starts to fail reconstruction with lower  $SNR_y$ .

Algorithm	$SNR_y$ 0 dB		$SNR_y$ -5 dB		$SNR_y$ -10 dB		$SNR_y$ -15 dB	
	SNR	Loss	SNR	Loss	SNR	Loss	SNR	Loss
FBP	4.50	1182.3	-0.31	1982.2	-5.25	3454.1	-10.22	6101.7
BM3D-sino	9.93	714.2	7.42	892.2	4.61	1179.8	<b>2.00</b>	<b>1570.1</b>
BM3D-reco	<b>10.79</b>	<b>664.5</b>	<b>8.09</b>	<b>833.6</b>	<b>4.97</b>	<b>1137.7</b>	1.54	1677.5
U-Net	7.13	977.7	6.18	1054.1	4.34	1235.0	1.87	1545.4

Table 6.1: Small Scale Experiment: Baseline results.

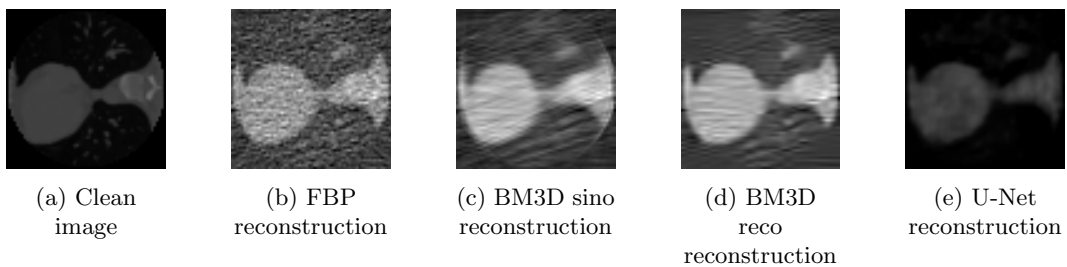


Figure 6.2: Sample reconstruction for baseline algorithms and  $SNR_y$  0 dB.

### 6.3.2 K-NN Experiments

In the following section, experiments with different input graphs are presented. Therefore, some other parameters are fixed for all experiments. GAT-Denoiser has been set to 3 layers with GAT single head and convolution. Noise was added to reach  $SNR_y$  0 dB. The input graph structure is important for GAT learning. In our case, the input graph was fixed after examination of GL embedding. Moreover, learning is expected to fail on a random graph.

**Does learning fail with a random graph?** Yes it does.

During this experiment, two models with different input graphs, but same number of nodes 1024 have been trained. First, a k-NN graph with  $k = 10$  was defined as input, therefore, around 1% of all nodes are connected in the graph. Second, a random Erdős–Rényi graph with  $p = 0.01$  has been evaluated, where every node is connected to every other node with probability  $p$ . As a consequence, nodes are approximately connected to 1% of all available nodes as well and evaluation should allow a fair comparison.

Table 6.2 shows Loss and SNR and in Figure 6.3 example reconstruction is illustrated. In the reconstruction from Erdős–Rényi graph, no details are captured (6.3(b)) and it clearly failed. The reconstruction quality of GAT-Denoiser in Figure 6.3(c) is rather low. However, it starts learning a few coarse details and with the upcoming experiments, the reconstruction can hopefully be increased in quality. But, our approach to define the input graph, based on the assumption of the underlying low-dimensional manifold to be on a circle, is reasonable.

Input graph	Loss	SNR
Erdős–Rényi graph with $p = 0.01$	1267.16	3.65
k-NN graph with $k = 10$	<b>804.7</b>	<b>7.3</b>

Table 6.2: Small Scale Experiment: Loss and SNR for random graph vs. k-NN graph.

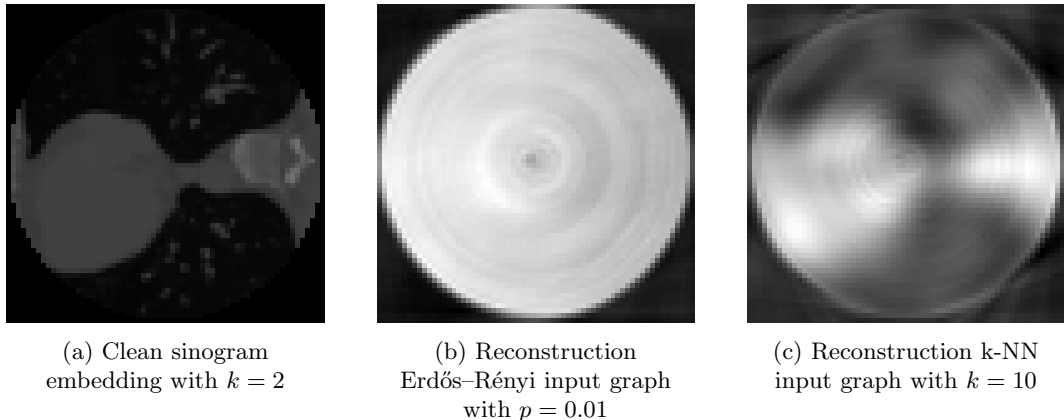


Figure 6.3: Reconstructions for different input graphs.

**Does result improve with more observations?** Yes. For this question to answer, multiple models have been trained for graphs with 512, 1024 and 2048 observations as well as different  $k = (2, 6, 8, 10, 20)$ . In Table 6.3 results are presented, where results are averaged by the number of observations for different  $k$ . A larger number of nodes can improve the models. But, training is also more expensive regarding execution time. Therefore, for all upcoming experiments number of observations is fixed to 1024, as it looks like a good value in between, with good reconstruction results but also not too much training time.

Number of observations	SNR	Loss	Training time (s)
512	7.22	822.6	2678.6 s
1024	<b>7.80</b>	<b>766.9</b>	<b>4216.1 s</b>
2048	8.55	701.5	7609.0 s

Table 6.3: Small Scale Experiment: Loss and SNR for different number of observations averaged by  $k$ .

**What is a good value for  $k$ ?** To find suitable  $k$ , multiple models have been trained with different  $k = (1, 2, 3, 4, 6, 8, 10, 20)$  as well as different  $\text{SNR}_y$  (0 dB and -10 dB). In Table 6.4 the results of the evaluated models are presented. For  $\text{SNR}_y$  0 dB the best result can be achieved with  $k = 2$  and for  $\text{SNR}_y$  -10 dB  $k = 1$ . With our assumption of fixed angles, and 1024 observations, it looks like only a few neighbors are enough to capture important information in the neighborhood.

k	$\text{SNR}_y$ 0 dB		$\text{SNR}_y$ -10 dB	
	SNR	Loss	SNR	Loss
1	8.81	678.7	<b>7.09</b>	<b>827.5</b>
2	<b>9.16</b>	<b>652.4</b>	6.95	849.4
3	8.64	689.2	6.38	912.7
4	8.37	712.4	6.29	906.8
6	8.25	722.8	5.81	958.3
8	7.99	744.1	5.64	985.8
10	7.30	804.7	5.54	996.3
20	6.30	910.5	4.82	1090.6

Table 6.4: Small Scale Experiment: Different  $k$  values for  $\text{SNR}_y$  0 dB and -10 dB.

### 6.3.3 GAT Experiments

In this section, experiments are presented with a focus on the GAT and its parameters. Mainly, two parameters are of interest: number of heads and number of layers. Number of layers is expected to keep rather low, as it defines the exposure of the k-hop neighborhood. The observations have only resolution 64x64 and consequently, it is expected that too many layers will average a too large neighborhood. Further, the number of heads determines if the learned weight matrix is divided into several parts. The larger the number of heads, the smaller are the parts of the weight matrix. Overall, a larger number of heads is expected to smoothen denoising, but too large values will divide weight matrix in too many parts, leading to bad results.

Experiments have been computed in parallel and the results for the k-NN experiments have not been available. Therefore, graphs were constructed with  $k = 8$ , even though it is not the best value for  $k$ . Further, multiple experiments with layers = (2, 3, 4, 6) and heads = (1, 2, 4, 8, 16) have been evaluated. Results are illustrated in Table 6.5.

Heads	2 Layers		3 Layers		4 Layers		6 Layers		Average	
	SNR	Loss	SNR	Loss	SNR	Loss	SNR	Loss	SNR	Loss
1	7.55	784.2	6.65	869.1	<b>6.08</b>	<b>934.2</b>	3.19	1334.1	5.87	980.4
2	7.88	753.4	7.17	821.7	5.98	958.8	3.55	1256.5	<b>6.15</b>	<b>947.6</b>
4	8.22	727.6	6.26	927.4	4.10	1176.1	<b>4.08</b>	<b>1191.2</b>	5.67	1005.6
8	8.14	732.3	<b>7.28</b>	<b>808.1</b>	5.54	1010.4	2.81	1516.2	5.94	1016.7
16	<b>8.27</b>	<b>721.9</b>	5.69	990.5	5.98	941.8	2.81	1516.0	5.66	1042.6
Average	8.01	743.9	6.59	883.4	5.54	1004.3	3.29	1362.8		

Table 6.5: Small Scale Experiment: Different GAT parameters.

**The more layers the better result?** No. As expected, when working with too many layers, denoising starts failing as it averages over a neighborhood, which is too large. In Table 6.5, 6 layers clearly get the worst result, followed by 4, 3 and 2 layers.

**How do multiple heads affect the result?** It has an overall positive impact. During experiments, for every layer  $l$  with single-head, there is a better result for  $l$ , where multiple-heads are applied. For  $l = 2$ , single-head model performs with an average SNR of 7.55 dB where with 16 heads average SNR is 8.27.

2 layers seems to be most promising and number of heads 4 seems to be a reasonable choice for heads. With 16 heads, the result was even a bit better. As 16 heads performed rather low for other number of layers, the best GAT parameters for the LoDoPaB-CT dataset are considered to be 2 layers and 4 heads. To make sure that  $k = 2$  is a good setting for these GAT parameters, the k-NN experiment has been recomputed for 2 layers and 4 heads. Table D.2 presents results, which give the same insight as the previous k-NN experiments.

**How about some dropout?** An experiment with fixed network parameters and different dropout values (0, 0.01, 0.03, 0.05, 0.1) has been computed. Results are presented in Figure D.3. There is not too much of a difference. Without dropout, model got the best value, followed by 0.05 and 0.03 with almost the same result.

Therefore, in future trainings, dropout of 0.05 was used.

### 6.3.4 Convolution Experiments

For convolution, kernel size and padding can be defined. Moreover, it is possible to increase number of channels during convolution. For GAT, the number of layers determines the averaging neighborhood. As multiple channels are expected to perform better with multiple layers, there could be a trade-off between GAT quality (size of averaging neighborhood) and convolution quality (increasing number of channels).

First, some experiments with 4 layers and 2 heads have been executed with different number of kernel, padding and number of channels. The aim is to find good convolution kernel and padding parameter values.

**What is a good kernel size?** In Table 6.6 results are illustrated. Best results are achieved with only 1 channel and smallest kernel size of 3 with padding 1. This is not too big of a surprise, observation dimension is only 64 and, therefore, a smaller kernel size make sense.

Kernel and Padding	1 Channel		4 Channel		8 Channel		16 Channel	
	SNR	Loss	SNR	Loss	SNR	Loss	SNR	Loss
7 / 3	3.56	1328.7	4.60	1330.0	<b>3.76</b>	<b>1363.4</b>	<b>2.81</b>	<b>1515.7</b>
5 / 3	4.94	1081.0	2.76	1548.5	2.66	1597.0	<b>2.81</b>	<b>1515.7</b>
3 / 1	<b>6.49</b>	<b>900.6</b>	<b>5.06</b>	<b>1084.8</b>	1.30	2336.1	0.05	2844.4

Table 6.6: Small Scale Experiment: Convolution for GAT-Denoiser with 4 layers and 2 heads.

**Is there a trade-off between GAT and Convolution?** As kernel size 3 with padding 1 seems to be a good value for the LoDoPaB-CT dataset, in the second convolution experiment different GAT architectures are compared with kernel size 3. Good performing GAT architectures for layers 2 to 4 have been chosen: 2 layers with 4 heads, 3 layers with 8 heads and 4 layers with 2 heads.

The resulting evaluation is illustrated in Table 6.7. Additionally, for every GAT architecture model without convolution has been computed. For every architecture, there was a model with convolution which performed better than the one without convolution.

Convolution can be considered to contribute to the success of GAT-Denoiser.

Channels	2 Layers		3 Layers		4 Layers	
	SNR	Loss	SNR	Loss	SNR	Loss
No Conv	6.99	839.3	4.31	1175.5	<b>6.91</b>	<b>842.2</b>
1	<b>8.10</b>	<b>735.6</b>	6.91	<b>842.2</b>	6.49	900.6
4	7.12	834.6	6.45	903.0	5.06	1084.8
8	<b>7.79</b>	<b>767.3</b>	<b>7.01</b>	862.9	1.30	2336.1
16	7.45	798.8	5.97	1002.9	0.05	2844.4

Table 6.7: Small Scale Experiment: Convolution for GAT-Denoiser with different number of layers and heads.

### 6.3.5 Loss Experiments

An experiment was set up to compare  $\mathcal{L}$  from Equation 5.4 with  $\mathcal{L}_{sino}$  from Equation 5.3. The same network parameters have been used, but once loss during training was defined with  $\mathcal{L}$  and once  $\mathcal{L}_{sino}$ . The experiments have been computed for  $\text{SNR}_y$  0, -5, -10 and -15 dB.

**Is end-to-end learning a good idea?** Yes, but it comes with a price. Averaged results over training loss can be found in Table 6.8. Overall, the models trained with loss  $\mathcal{L}$  performed around 0.8 dB in SNR better. But, training of the network took much longer, more than factor 3. This is not a big surprise. For learning with  $\mathcal{L}$ , reconstruction of every sample needs to be done in every epoch, where for  $\mathcal{L}_{sino}$  reconstruction can be omitted.

End-to-end learning with loss  $\mathcal{L}$  contributes to the success of GAT-Denoiser and is used in further experiments.

Loss training	Average SNR	Average Loss	Training time (s)
$\mathcal{L}$	<b>7.29</b>	<b>816.7</b>	3812 s
$\mathcal{L}_{sino}$	6.49	981.3	<b>1209 s</b>

Table 6.8: Small Scale Experiment: Average Loss and SNR of training loss  $\mathcal{L}$  and  $\mathcal{L}_{sino}$ .

### 6.3.6 GAT-Denoiser Component Experiments

The final small scale experiments aim to see contribution of the single components in action. Therefore, a fixed overall architecture is defined and experiments with different combination of components (Convolution, GAT and U-Net) will be calculated. Further, models with joint U-Net training have been evaluated. The fixed settings for GAT-Denoiser have been defined with 2 layers, 4 heads, convolution with kernel size 3 and padding 1.  $k$  was set to 2. Overall, 8 models have been evaluated and compared against the baseline algorithms for  $\text{SNR}_y = (-15, -10, -5, 0)$  dB.

Results are plotted in Figure 6.4 and numeric values can be found in Table D.1. First, *GAT* is the model, where no convolution and no U-Net is active. Second, *GAT+Conv* refers to the model with GAT and convolution but no U-Net. Additionally, the two models have

been combined with U-Net, which are referred to as *GAT+U-Net* and *Conv+GAT+U-Net*. Last, models with joint U-Net training are presented. *U-Net\** denotes that during all 200 epochs U-Net is jointly trained. *U-Net\*\** denotes that during the first 100 epochs U-Net is kept static and in the second 100 epochs joint training is applied.

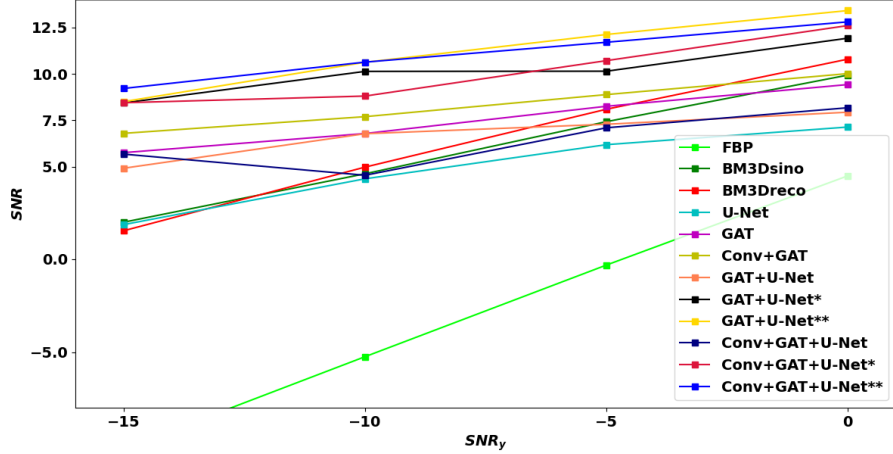


Figure 6.4: Small Scale Experiments: Reconstruction SNR of different GAT-Denoiser models and baseline algorithms.

Model *GAT* is not able to beat baseline algorithms, and it seems that only applying GAT is not enough. *GAT+Conv* performs slightly better. When adding U-Net in the models *GAT+U-Net* and *Conv+GAT+U-Net*, the visual results improve slightly, but reconstruction SNR is still not able to beat baseline algorithms. Finally, with joint training of GAT-Denoiser and U-Net, results can beat baseline algorithms for the small scale experiment. It was helpful, to first train only GAT-Denoiser for 100 epochs and start joint training for the second 100 epochs.

Figure 6.5 illustrates visual results for all baseline algorithms and some GAT-Denoiser models. Further, clean sample is presented in Figure 6.5(a).

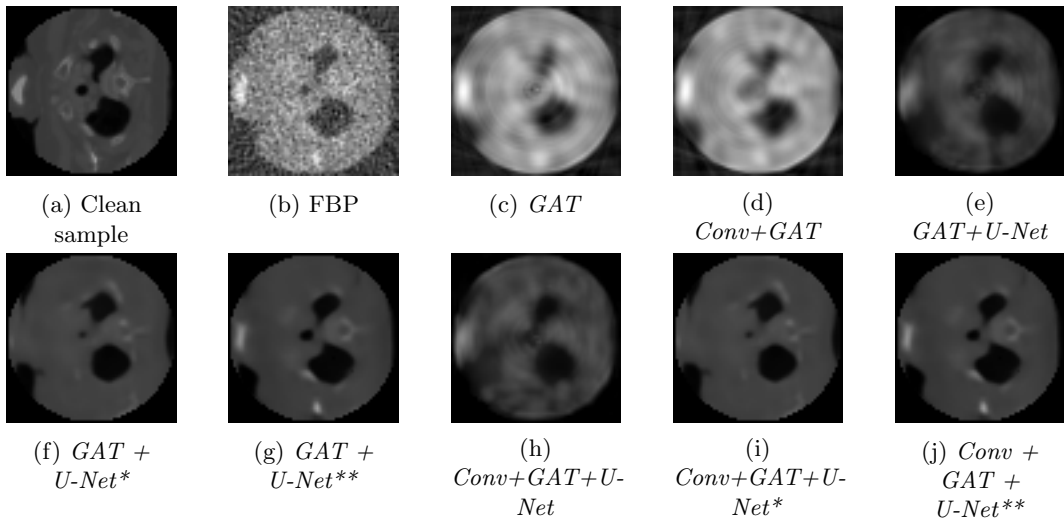


Figure 6.5: Small Scale Experiment: Visual results for  $\text{SNR}_y$  0 dB.

## 6.4 Large Scale Experiments

In this section, large scale experiments are presented, which have been trained on the complete LoDoPaB-CT dataset as well as evaluated on the complete LoDoPaB-CT test dataset. From last section, the most promising parameters for the GAT-Denoiser architecture have been chosen to find the best model. The following parameters have been fixed during the large scale experiments:  $k = 2$ , number of layers = 2, number of heads = 4, convolution with kernel size 3 and padding 1. The GAT-Denoiser models have been trained for 20 epochs, if not mentioned differently. Wandb experiment results can be found in Appendix D.6.

### 6.4.1 Baseline

In Table D.4, baseline results for the large scale experiment can be found. As only the number of samples changed, but algorithms are fixed, the result is roughly the same as for the small scale experiments.

### 6.4.2 GAT-Denoiser Components Experiments

The main components of the GAT-Denoiser pipeline have been tested with different models. As a result of the small scale experiments, joint U-Net training was most promising, when there was first training on GAT-Denoiser solely and in a second step joint training. Therefore, model Conv + GAT + U-Net\* and GAT+U-Net\* is omitted for the large scale experiments. Moreover, ... U-Net\*\* denotes that models have been first trained 10 epochs with static U-Net and after with joint U-Net training.

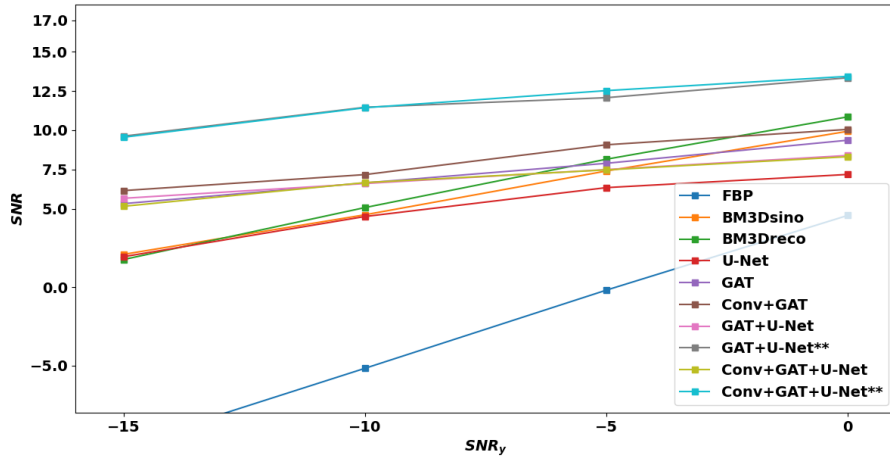


Figure 6.6: Large Scale Experiments: Reconstruction SNR of different GAT-Denoiser models and baseline algorithms.

Figure 6.6 presents resulting SNR for baseline algorithms and different GAT-Denoiser models. Further, numerical results are presented in Table D.5. The results are rather similar compared to the small scale experiments. Overall reconstruction is slightly better, as during training more samples have been seen. Again, approaches with joint U-Net and GAT-Denoiser training performed best.

#### 6.4.3 Best Models Experiments

For the most promising architectures, the models have been further trained for 20 epochs. In Table 6.9 final results are illustrated. The number in brackets denotes the number of training epochs with static U-Net followed by the number of epochs with joint training. All in all, a few more epochs could sometimes improve the result, as for *Conv+GAT+U-Net* and  $SNR_y$  0 dB. Although, this is not always the case, and in some scenarios the model even performed worse, as for *GAT+U-Net* and  $SNR_y$  -10 dB.

Model	$SNR_y$ 0 dB		$SNR_y$ -5 dB		$SNR_y$ -10 dB		$SNR_y$ -15 dB	
	SNR	Loss	SNR	Loss	SNR	Loss	SNR	Loss
GAT+U-Net(10/10)	13.34	413.8	12.07	469.2	<b>11.46</b>	<b>502.0</b>	9.62	633.5
GAT+U-Net(10/30)	<b>13.43</b>	<b>406.2</b>	<b>12.85</b>	<b>428.2</b>	10.83	546.2	9.65	<b>603.3</b>
GAT+U-Net(20/20)	13.16	412.2	12.10	469.9	11.02	529.0	<b>10.0</b>	606.0
Conv+GAT+U-Net(10/10)	13.43	403.5	12.52	450.1	<b>11.43</b>	509.9	9.55	638.0
Conv+GAT+U-Net(10/30)	13.68	395.4	12.32	460.3	11.40	<b>509.1</b>	9.25	688.1
Conv+GAT+U-Net(20/20)	<b>13.87</b>	<b>385.4</b>	<b>12.81</b>	<b>442.3</b>	10.90	547.5	<b>10.1</b>	<b>604.4</b>

Table 6.9: Large Scale Experiment: Baseline results.

A single sample reconstruction for  $SNR_y$  0 dB is presented in Figure 6.7. Additional visual results are presented in the Appendix D.5 for baseline algorithms and the best performing large scale GAT-Denoiser models for different  $SNR_y$ .

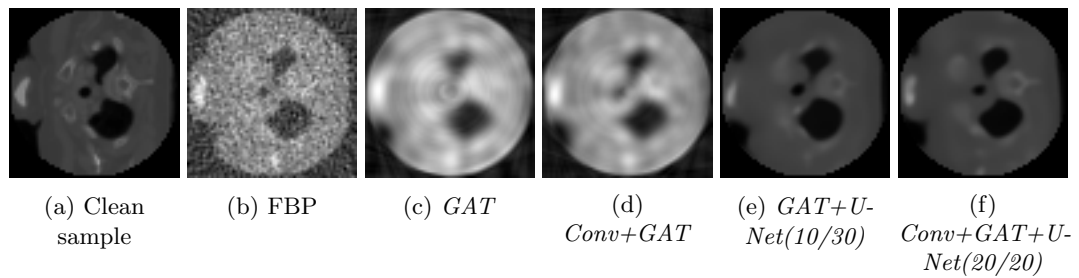


Figure 6.7: Large Scale Experiment: Visual results for  $\text{SNR}_y$  0 dB.

# 7

## Conclusion and Future Work

In this final chapter, the conclusion and future work is presented.

### 7.1 Conclusion

In this Thesis, the molecular imaging methods CT and Cryo-EM within the high noise domain, have been the problems to approach.

During the practical part, 2D and 3D tomography have been implemented in python to familiarize with the domain. Further, vector diffusion map was implemented in 3D to do some comparison and code was integrated with Aspire<sup>12</sup>. Finally, GAT was implemented and further optimized with convolution and U-Net. Finally, GAT-Denoiser is derived.

During evaluation on the LoDoPab-CT dataset, baseline algorithm BM3D was implemented. Overall, GAT-Denoiser shows great results and improves reconstruction SNR by 379.9%, 126.0% 57.7%, 27.6% for  $\text{SNR}_y$  -15 dB, -10 dB, -5 dB and 0 dB. GAT-Denoiser is able to capture important observation information even in the high-noise domain. Moreover, the individual components contribute to the success of GAT-Denoiser. With the small scale experiments, it was shown that convolution, GAT and the end-to-end learning approach are all valuable individually and are therefore well-chosen. Additionally, the large scale experiments found the best GAT-Denoiser model. GAT-Denoiser combined with U-Net and joint neural network training can upgrade CT reconstruction in the high-noise domain to a new level.

### 7.2 Future Work

Cryo-EM is an open research area of great interest. The 3D problem is not easy to solve and there are many steps in the Cryo-EM reconstruction pipeline to be further improved. With GAT-Denoiser, a neural network architecture is introduced, towards an algorithm to work for Cryo-EM

---

<sup>12</sup> <http://spr.math.princeton.edu/>

**Improve GAT-Denoiser:** The current GAT-Denoiser is not perfect. In the architecture, a single convolutional layer proceeds a single GAT layer. In some scenarios, it could be beneficial, to apply multiple convolutional layers before GAT and on could resolve the current architecture to allow multiple convolutional layer before GAT. Further, on could think of integrating convolution in GAT directly or adjust the architecture in other manners.

**GAT-Denoiser in 3D:** So far, GAT-Denoiser was evaluated on a CT dataset in 2D. Therefore, the next step would be to increase the dimension and derive GAT-Denoiser to work in 3D. This should be feasible without too much of an effort, as the single components of GAT-Denoiser are able to work in 3D as well. However, more resources will be needed for computation.

**Drop known Angle Assumption:** So far, GAT-Denoiser works with the assumption that angles are fixed. In a future work, this assumption could be dropped. GL embedding is a way to approximate angles for CT and Cryo-EM observations, but the quality in the high noise regime is rather low. To extend GAT-Denoiser to work with unknown angles, it needs to be combined with an additional component, which can successfully approximate angles in the high noise regime.

**Further Cryo-EM Challenges:** In this Thesis, only single particle Cryo-EM is considered. When GAT-Denoiser is available in 3D, one could think of an approach where from a given observation, the underlying sample is not structural equivalent and there are some slight differences. One needs to approximate the distribution of the underlying samples. This could be established first for known observation angles and further brought to unknown observation angles.

## Bibliography

- [1] Tamir Bendory, Alberto Bartesaghi, and Amit Singer. Single-particle cryo-electron microscopy: Mathematical theory, computational challenges, and opportunities. *IEEE Signal Processing Magazine*, 37(2):58–76, 2020. doi: 10.1109/MSP.2019.2957822.
- [2] David J Brenner and Eric J Hall. Computed tomography—an increasing source of radiation exposure. *New England journal of medicine*, 357(22):2277–2284, 2007. doi: 10.1056/NEJMra072149.
- [3] Antoni Buades, Bartomeu Coll, and J-M Morel. A non-local algorithm for image denoising. In *2005 IEEE Computer Society Conference on Computer Vision and Pattern Recognition (CVPR’05)*, volume 2, pages 60–65. IEEE, 2005. doi: 10.1109/CVPR.2005.38.
- [4] Lawrence Cayton. Algorithms for manifold learning. *Univ. of California at San Diego Tech. Rep*, 12(1-17):1, 2005.
- [5] Rolf Clackdoyle and Michel Defrise. Tomographic reconstruction in the 21st century. *IEEE Signal Processing Magazine*, 27(4):60–80, 2010. doi: 10.1109/MSP.2010.936743.
- [6] Ronald R Coifman and Stéphane Lafon. Diffusion maps. *Applied and computational harmonic analysis*, 21(1):5–30, 2006. doi: 10.1016/j.acha.2006.04.006.
- [7] Ronald R Coifman, Yoel Shkolnisky, Fred J Sigworth, and Amit Singer. Graph laplacian tomography from unknown random projections. *IEEE Transactions on Image Processing*, 17(10):1891–1899, 2008. doi: 10.1109/TIP.2008.2002305.
- [8] Kostadin Dabov, Alessandro Foi, Vladimir Katkovnik, and Karen Egiazarian. Image denoising by sparse 3-d transform-domain collaborative filtering. *IEEE Transactions on Image Processing*, 16(8):2080–2095, 2007. doi: 10.1109/TIP.2007.901238.
- [9] Allison Doerr. Single-particle cryo-electron microscopy. *Nature methods*, 13(1):23–23, 2016. doi: 10.1038/nmeth.3700.
- [10] Yifeng Fan and Zhizhen Zhao. Multi-frequency vector diffusion maps. In *International Conference on Machine Learning*, pages 1843–1852. PMLR, 2019. doi: 10.1109/cpa.21395.
- [11] Yifeng Fan and Zhizhen Zhao. Cryo-electron microscopy image denoising using multi-frequency vector diffusion maps. In *2021 IEEE International Conference on Image Processing (ICIP)*, pages 3463–3467. IEEE, 2021. doi: 10.1109/ICIP42928.2021.9506435.

- [12] Marco Gori, Gabriele Monfardini, and Franco Scarselli. A new model for learning in graph domains. In *Proceedings. 2005 IEEE International Joint Conference on Neural Networks, 2005.*, volume 2, pages 729–734. IEEE, 2005. doi: 10.1109/IJCNN.2005.1555942.
- [13] Diederik P Kingma and Jimmy Ba. Adam: A method for stochastic optimization. *arXiv preprint arXiv:1412.6980*, 2014. doi: 10.48550/arXiv.1412.6980.
- [14] Thomas N Kipf and Max Welling. Semi-supervised classification with graph convolutional networks. *arXiv preprint arXiv:1609.02907*, 2016. doi: 10.48550/arXiv.1609.02907.
- [15] Johannes Leuschner, Maximilian Schmidt, Daniel Otero Baguer, and Peter Maaß. The lodopab-ct dataset: A benchmark dataset for low-dose ct reconstruction methods. *arXiv preprint arXiv:1910.01113*, 2019. doi: 10.1038/s41597-021-00893-z.
- [16] Johannes Leuschner, Maximilian Schmidt, Poulami Somanya Ganguly, Vladyslav Andriashen, Sophia Bethany Coban, Alexander Denker, Dominik Bauer, Amir Hadjifaradji, Kees Joost Batenburg, Peter Maass, et al. Quantitative comparison of deep learning-based image reconstruction methods for low-dose and sparse-angle ct applications. *Journal of Imaging*, 7(3):44, 2021. doi: 10.3390/jimaging7030044.
- [17] Olaf Ronneberger, Philipp Fischer, and Thomas Brox. U-net: Convolutional networks for biomedical image segmentation. In *International Conference on Medical image computing and computer-assisted intervention*, pages 234–241. Springer, 2015. doi: 10.1007/978-3-319-24574-4\_28.
- [18] Amit Singer. Mathematics for cryo-electron microscopy. In *Proceedings. of the International Congress of Mathematicians: Rio de Janeiro 2018*, pages 3995–4014. World Scientific, 2018. doi: 10.1142/9789813272880\_0209.
- [19] Amit Singer and H-T Wu. Vector diffusion maps and the connection laplacian. *Communications on pure and applied mathematics*, 65(8):1067–1144, 2012. doi: 10.1002/cpa.21395.
- [20] Daniel Spielman. Spectral graph theory. *Combinatorial scientific computing*, 18, 2012. doi: 10.1201/b11644-19.
- [21] Peter Toft. The radon transform. *Theory and Implementation (Ph. D. Dissertation)(Copenhagen: Technical University of Denmark)*, 1996.
- [22] Ashish Vaswani, Noam Shazeer, Niki Parmar, Jakob Uszkoreit, Llion Jones, Aidan N Gomez, Łukasz Kaiser, and Illia Polosukhin. Attention is all you need. *Advances in neural information processing systems*, 30, 2017. doi: 10.48550/arXiv.1706.03762.
- [23] Petar Veličković, Guillem Cucurull, Arantxa Casanova, Adriana Romero, Pietro Lio, and Yoshua Bengio. Graph attention networks. *arXiv preprint arXiv:1710.10903*, 2017. doi: 10.48550/arXiv.1710.10903.

- [24] Ulrike Von Luxburg. A tutorial on spectral clustering. *Statistics and Computing*, 17(4):395–416, 2007. doi: 10.1007/s11222-007-9033-z.
- [25] Yue Wang, Yongbin Sun, Ziwei Liu, Sanjay E Sarma, Michael M Bronstein, and Justin M Solomon. Dynamic graph cnn for learning on point clouds. *Acm Transactions On Graphics (tog)*, 38(5):1–12, 2019. doi: 10.1145/3326362.
- [26] Felix Wu, Amauri Souza, Tianyi Zhang, Christopher Fifty, Tao Yu, and Kilian Weinberger. Simplifying graph convolutional networks. In *International Conference on Machine Learning*, pages 6861–6871. PMLR, 2019. doi: 10.48550/arXiv.1902.07153.

# A

## Mathematical Tools

Some mathematical tools will be introduced in the following chapter.

### A.1 3D Rotation Matrix

A rotation matrix is a transformation matrix used to perform rotations. In the 3D case, matrix for rotating one single axis can be described as:

$$R_{e_x}(\theta) \begin{bmatrix} 1 & 0 & 0 \\ 0 & \cos \theta & -\sin \theta \\ 0 & \sin \theta & \cos \theta \end{bmatrix} \quad (\text{A.1})$$

$$R_{e_y}(\theta) \begin{bmatrix} \cos \theta & 0 & \sin \theta \\ 0 & 1 & 0 \\ -\sin \theta & 0 & \cos \theta \end{bmatrix} \quad (\text{A.2})$$

$$R_{e_z}(\theta) \begin{bmatrix} \cos \theta & -\sin \theta & 0 \\ \sin \theta & \cos \theta & 0 \\ 0 & 0 & 1 \end{bmatrix} \quad (\text{A.3})$$

Where  $e_x, e_y, e_z$  corresponds to the axis unit-vector (for x:  $(1, 0, 0)$ , etc.) and  $\theta \in \mathbb{R}$ . To combine the single axis rotations, matrices can be multiplied with each other:

$$R(\theta) = R_{e_x}(\theta)R_{e_y}(\theta)R_{e_z}(\theta) \quad (\text{A.4})$$

In Equation A.4, angle  $\theta$  is the same for all axis, which does not have to be.

### A.2 Power Iterations

Power iteration, also called power method, is an iterative algorithm that approximates the largest eigenvalue of a diagonalizable matrix  $A$ .

The algorithm starts with a random vector  $b_0$  or an approximation of the dominant eigenvector.

$$b_{k+1} = \frac{Ab_k}{\|Ab_k\|} \quad (\text{A.5})$$

It will not necessarily converge. It only converges if  $A$  has an eigenvalue strictly greater than its other eigenvalues and initial vector  $b_0$  is not orthogonal to the eigenvector associated with the largest eigenvalue.

# B

## Graph Laplacian Embedding

In the following section, an introduction to manifolds and the GL embedding is given.

### B.1 Manifolds

The manifold assumption is a popular assumption for high-dimensional datasets. For a given dataset in high-dimension, one can assume that data points are samples drawn from a low-dimensional manifold, that embeds the high-dimensional space. Therefore, if the underlying manifold can be approximated, a dimensionality reduction is established as one can embed data points in the low-dimensional manifold space. There is a complete area of research devoted to this manifold assumption called Manifold Learning [4].

For high-dimensional data Euclidean distances are not meaningful in the sense that they will not capture similar data points well. GL can be used to compute a low-dimensional embedding which can map from high-dimensional space to the low-dimensional space. In the low-dimensional space, Euclidean distances make sense again.

**Definition:** Let manifold  $M$  be defined as  $\mathcal{M} = \{f(x), f \in C^K, f : \mathbb{R}^D \rightarrow \mathbb{R}^d\}$ . In this Thesis, only  $C^k$  differentiable d-dimensional manifolds defined by  $\mathcal{M}$  are considered. When  $d \ll D$ , the manifold defines a low-dimensional embedding, which maps from high-dimensional space  $\mathbb{R}^D$  to low-dimensional space  $\mathbb{R}^d$ .

Let's give two popular examples of manifolds, namely the *circle* and the *sphere*. The circle is a 1D manifold, where  $d = 1$  and  $D = 2$ . A sphere is a 2D manifold with  $d = 2$  and  $D = 3$ . In Figure B.1(a), 200 samples are drawn from a uniform distribution of the unit-circle manifold and in Figure B.1(b), 800 samples are drawn from a uniform distribution of the unit-sphere manifold, as well as the sphere itself.

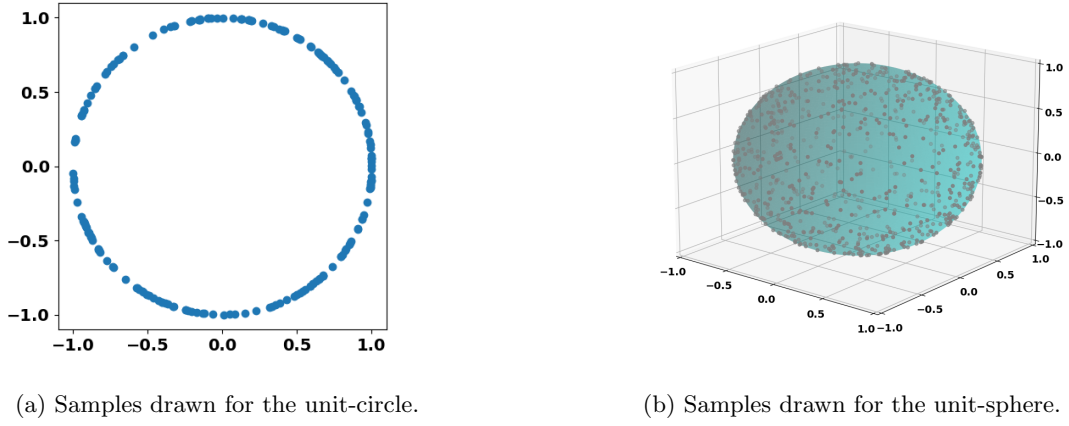


Figure B.1: Samples drawn from a 1D and 2D manifold.

**Graph Laplacian Embedding:** A low-dimensional embedding of a dataset can be computed with GL by the following:

1. Construct the k-NN graph from the dataset
2. Calculate the GL
3. Extract the second, third (and fourth) smallest eigenvectors

Another popular algorithm for calculating a low-dimensional embedding is diffusion maps [6], which is a non-linear approach using GL. Vector diffusion maps [19] generalize the concept of diffusion maps for vector fields. Multi-frequency vector diffusion maps [10] can be seen as an extension to vector diffusion maps, which works well even on highly noisy environments. Fan and Zhao [11] successfully applied multi-frequency vector diffusion Maps in Cryo-EM setting, where it was used for denoising observations.

### B.1.1 Embedding Quality

Finding a good embedding is not trivial, and in our case, the embedding is dependent on  $k$  during graph construction as well as parameter  $\theta$ ,  $s$  and  $\eta$ .

$k$  is an important parameter for building up a graph. If set too low, neighbors do not capture similar data well as too few nodes are connected. Further, if  $k$  is set too high, power of a neighbor is weakened and data is not well explained. In Figure B.2(a), the GL embedding computed from clean sinogram and  $k$  from 2 to 10 is illustrated. From  $k \leq 4$  the GL embedding approximates a circle and with  $k > 4$  it moves further away from the circle. If data is noisy, it is expected to be harder to construct a meaningful GL embedding, as some connections within the graph will be noisy. This is exactly what is illustrated in Figure B.2(b), where different GL embedding for noisy sinogram with  $\text{SNR}_y = 20$  dB and  $k$  from 3 to 10 are illustrated. GL embedding can never express data with a perfect circle. As noise is chosen rather moderate, GL embedding has still some power to express underlying data and is expected to decrease, if noise is increased.

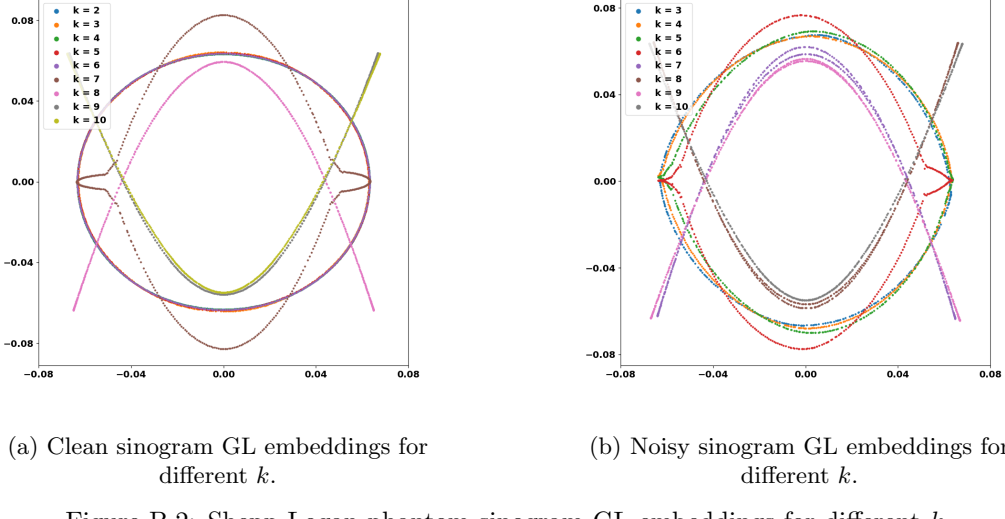


Figure B.2: Shepp-Logan phantom sinogram GL embeddings for different  $k$ .

While observing a sinogram,  $\theta$  defines how many observations (straight lines) are drawn and  $\text{dim}(s)$  defines the number of sampling points. Both have a great impact to expressiveness of our sinogram. In Figure B.3(a) GL embedding with  $\theta \in \mathbb{R}^{200}$  and  $k=6$  is illustrated for clean sinogram. It looks like 6 are too many neighbors, as the perfect circle cannot be established anymore. But, if  $\theta$  is increased to  $\theta \in \mathbb{R}^{500}$ , more nodes are available to choose good neighbors from and a circle can be established (Figure B.3(b)).

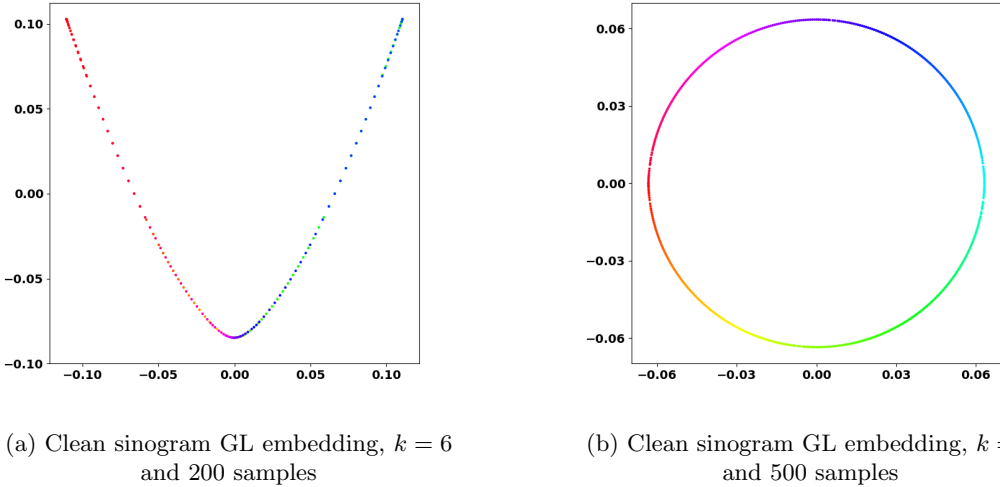
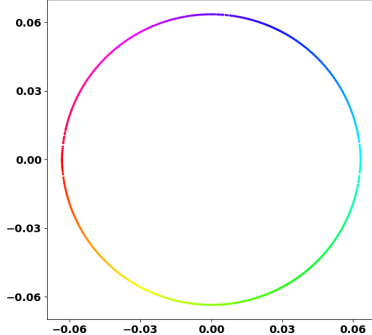


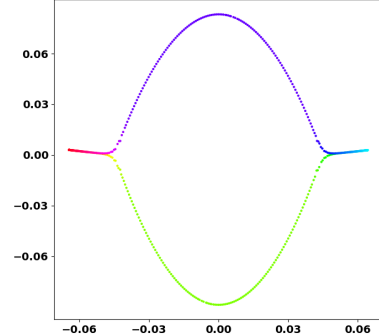
Figure B.3: Shepp-Logan phantom sinogram GL embeddings: Importance of number of samples.

Moreover, the number of sampling points is important. The more sampling points available, it is expected to be harder to come up with good neighbors (fixing  $k$  and number of samples), as more data needs to be explained with the same amount of neighbors. It is more likely, that nodes are connected wrongly. This can be seen in Figure B.4(a) and Figure B.4(b),

where with  $\dim(s) = 200$ , the perfect circle can be established and with  $\dim(s) = 400$ , not anymore (by same parameter  $k = 6$  and  $\theta \in \mathbb{R}^{500}$ ).



(a) Clean sinogram GL embedding,  
 $k = 6$  and  $\dim(s) = 200$



(b) Clean sinogram GL embedding,  
 $k = 6$  and  $\dim(s) = 400$

Figure B.4: Shepp-Logan phantom sinogram GL embeddings: Importance of sample dimension.

Since the GL embedding is sensitive to  $k$ , it is best practice to try different values in order to find the best GL-manifold.

# C

## Neural Networks

In GAT-Denoiser, concepts from existing neural networks have been combined. In this chapter, GAT, Convolution and U-Net are introduced in detail.

### C.1 Graph Attention Networks

The main component of GAT-Denoiser is a GAT. GAT is an extension to GCN and adds attention (or weights) to neighbors for learning new node feature representations. Topology of the graph will not change but weighted averaging over the neighborhood will be computed.

**Single Layer:** The input of a single GAT layer are node features  $h = \{h_1, h_2, \dots, h_N\} \in \mathbb{R}^F$ , where  $N$  is the number of nodes and  $F$  the number of features per node. Single layer will map input to output, which can potentially have different dimensions:  $h' = \{h'_1, h'_2, \dots, h'_N\} \in \mathbb{R}^{F'}$ . As is other GNNs, input features are initially linearly transformed and parametrized by a learnable weight matrix  $W \in \mathbb{R}^{F' \times F}$ . This allows to add enough expressiveness to the neural network and weights are learned during training. Further, attention coefficients are computed, which indicates the importance of node  $j$  to node  $i$ :

$$e_{ij} = a(Wh_i, Wh_j) \quad (\text{C.1})$$

With  $a$  as the shared attentional mechanism  $a : \mathbb{R}^{F'} \times \mathbb{R}^{F'} \mapsto \mathbb{R}$ . Veličković et al. [23] proposed to use a single-layer feedforward neural network, parametrized by a weight vector  $a \in \mathbb{R}^{2F'}$  and LeakyReLU as activation function.

To compare coefficients  $e$  across different nodes, normalization is needed. Therefore, softmax is used as normalization  $\alpha_{ij} = \text{softmax}_j(e_{ij})$  such that all attention coefficients of a single node sum up to 1 and therefore, are nicely comparable across nodes. Finally, the new node embedding is calculated as:

$$h'_i = \sigma \left( \sum_{j \in \mathcal{N}_i} \alpha_{ij} Wh_j \right) \quad (\text{C.2})$$

With  $\sigma$  as some arbitrary activation function.

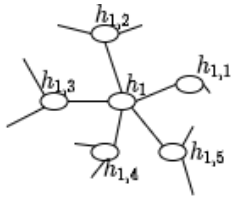


Figure C.1: GAT node feature propagation.

Figure C.1 shows how node features are propagated in the network. Node  $h_1$  has 5 neighbors and for a single GAT layer, new node feature  $h'_1$  is computed with Equation C.2:

$$h'_1 = \sigma \left( \sum_{i=1}^5 \alpha_i W h_{1,i} \right)$$

**Multi-Head Attention:** Motivated by the work of Vaswani et al. [22], multi-head attention can be beneficial to stabilize learning process. Therefore, not only a single weight matrix is learned, but  $W$  is split up in several parts, all learned individually:

$$h'_i = \parallel_{k=1}^K \sigma \left( \sum_{j \in \mathcal{N}_i} \alpha_{ij}^k W^k h_j \right) \quad (\text{C.3})$$

Where  $\parallel$  corresponds to concatenation,  $\alpha_{ij}^k$  the  $k$ -th attention mechanism and  $W^k$  the  $k$ -th linear transformations weight matrix. The final output consists of  $KF'$  output features.

**Last layer:** In the last layer, output dimension needs to be obtained. Consequently, concatenation is no longer plausible and averaging is used to match desired dimension.

## C.2 Convolution

Convolution is an important concept in Signal Processing, because it allows averaging of an incoming signal. Convolution commonly operators on pixel spaces, where every observation location or time slot gets one value assigned.

$$x * k = y \quad (\text{C.4})$$

Where  $x$  is the input signal,  $*$  convolution,  $k$  the kernel and  $y$  the convolved signal.

To apply convolution, a kernel with weights needs to be defined. This kernel will then slide over the input signal  $x$  and computes the dot product with its weights. Figure C.2 illustrates 1D convolution. Kernel size is set to 3,  $n$  refers to input signal size and  $m$  to output signal size. In the example  $n = m + 2$ , thus, the convolved output signal size will be decreased by 2. The concept of convolution can be extended to arbitrary dimensions.

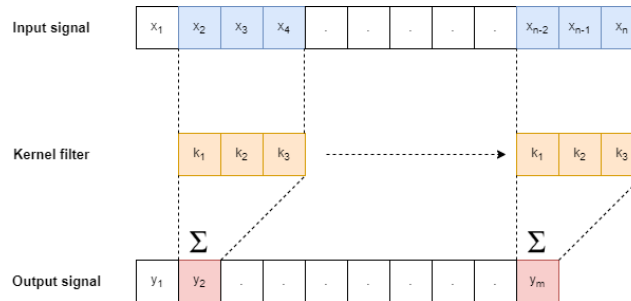


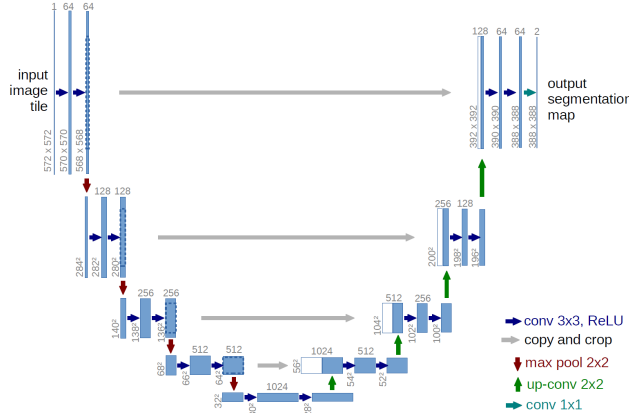
Figure C.2: 1D Convolution illustration.

**Padding:** Padding can be applied to add pixels to the boundary of the signal. In the example, padding is set to 0 and therefore, the signal size is decreased by 2. If signal size should be fixed during convolution, padding is a powerful tool. For padding 1, the input size  $n$  would be equal to output size  $m$ , as an extra element in the output signal will be at convolved at boundaries.

**Stride:** Stride is the parameter how far the kernel moves each step. In the example, stride was defined to be 1. If stride is increased, the output signal size will decrease.

### C.3 U-Net

U-Net can improve the performance of CT reconstruction, where FBP is further refined with a neural network. It is a convolutional neural network, which is well suited for image segmentation in different domains. The neural network architecture consists of a contracting path and a expansive path, resulting in a U-shape, as illustrated in Figure C.3.



Number on top of boxes denotes channels, where numbers at bottom of boxes refer to input dimension.

Figure C.3: U-Net architecture [17, p 2, Fig. 1].

During the contracting path (left part), the input dimension is decreased, but channels are increased. For every step in the contracting path, two 3x3 convolution layers are followed by ReLu and a 2x2 max pooling for down-sampling. Further, at each down-sampling step, the input channels are doubled. Multiple contracting steps are combined. After the last contracting step, expansive path (right part) starts where input dimension will be increased and input channels will be decreased. For every expansive step, an up-sampling of the feature map takes place, followed by a 2x2 convolution, which halves the number of channels. Then, concatenation with the corresponding feature map of the contracting path is done (gray arrow ), followed by again two 3x3 convolutions and ReLu. Final layer is a 1x1 convolution to map to desired output dimension and single output channel.

# D

## Additional Results

In this chapter, additional numeric and visual results are presented, that shall extend results presented in Chapter 6.

### D.1 Small Scale Experiment: GAT-Denoiser Components

Table D.1 shows numerical results for the small scale experiment. Results for the baseline algorithms, different models with  $k = 2$  and  $k = 8$  are presented.

Algorithm / Model	$\text{SNR}_y$ 0 dB SNR	$\text{SNR}_y$ -5 dB SNR	$\text{SNR}_y$ -10 dB SNR	$\text{SNR}_y$ -15 dB SNR
FBP	4.50	-0.31	-5.25	-10.22
BM3D sino	9.93	7.42	4.61	<b>2.00</b>
BM3D reco	<b>10.79</b>	<b>8.09</b>	<b>4.97</b>	1.54
U-Net	7.13	6.18	4.34	1.87
<b>k=2</b>				
GAT	9.42	8.25	6.78	5.75
Conv+GAT	10.01	8.88	7.69	6.79
GAT+U-Net	7.93	7.28	6.77	4.91
GAT+U-Net*	11.92	10.14	10.13	8.43
GAT+U-Net**	<b>13.41</b>	<b>12.12</b>	10.62	8.50
Conv+GAT+U-Net	8.17	7.09	4.53	5.67
Conv+GAT+U-Net*	12.60	10.71	8.80	8.44
Conv+GAT+U-Net**	12.80	11.70	<b>10.63</b>	<b>9.21</b>
<b>k=8</b>				
GAT	8.32	6.94	6.19	5.01
Conv+GAT	9.05	8.07	6.99	5.75
GAT+U-Net	7.49	6.40	6.01	5.07
GAT+U-Net**	11.88	<b>10.85</b>	<b>9.68</b>	<b>8.26</b>
Conv+GAT+U-Net	7.55	6.50	5.74	4.87
Conv+GAT+U-Net**	<b>11.94</b>	10.31	7.34	7.33

Table D.1: Small Scale Experiment: GAT-Denoiser components vs. baseline algorithms.

## D.2 Small Scale Experiment: Further k-NN Results

K-NN experiment with 2 layers and 4 heads can be found in Table D.2.

k	SNR <sub>y</sub> 0 dB	
	Loss	SNR
2	<b>9.90</b>	<b>601.4</b>
4	9.64	622.1
6	9.38	634.4
8	9.19	649.0

Table D.2: Small Scale Experiment: Different  $k$  values for SNR<sub>y</sub> 0 dB.

## D.3 Small Scale Experiment: GAT Dropout

Table D.3 presents results for experiments with different dropout values. GAT-Denoiser was defined with 2 layers and 4 heads.

GAT dropout	SNR <sub>y</sub> -5 dB	
	Loss	SNR
0	<b>8.33</b>	<b>739.5</b>
0.01	7.81	766.2
0.03	7.98	743.3
0.05	<b>8.09</b>	<b>738.4</b>
0.1	7.79	761.8

Table D.3: Small Scale Experiment: GAT dropout for SNR<sub>y</sub> -5 dB.

## D.4 Large Scale Experiment: Baseline Results

Table D.4 presents the result of the chosen baseline algorithms for the large scale experiment.

Algorithm	$\text{SNR}_y$ 0 dB		$\text{SNR}_y$ -5 dB		$\text{SNR}_y$ -10 dB		$\text{SNR}_y$ -15 dB	
	Loss	SNR	Loss	SNR	Loss	SNR	Loss	SNR
FBP	4.57	1167.6	-0.19	1973.5	-5.17	3425.3	-10.09	10'737.3
BM3D sino	9.93	709.9	7.40	890.6	4.61	1168.0	<b>2.09</b>	<b>1570.0</b>
BM3D reco	<b>10.85</b>	<b>658.2</b>	<b>8.15</b>	<b>818.6</b>	<b>5.07</b>	<b>1118.3</b>	1.76	1662.5
U-Net	7.18	968.8	6.34	1044.7	4.50	1214.1	1.94	1522.4

Table D.4: Large Scale Experiment: Baseline results.

### D.4.1 Large Scale Experiment: GAT-Denoiser Models

Table D.5 presents the final results for baseline algorithms and GAT-Denoiser models for the large scale.

Algorithm / Model	$\text{SNR}_y$ 0 dB SNR	$\text{SNR}_y$ -5 dB SNR	$\text{SNR}_y$ -10 dB SNR	$\text{SNR}_y$ -15 dB SNR
FBP	4.57	-0.19	-5.17	-10.09
BM3D sino	9.93	7.40	4.61	<b>2.09</b>
BM3D reco	<b>10.85</b>	<b>8.15</b>	<b>5.07</b>	1.76
U-Net	7.18	6.34	4.50	1.94
<b>k=2</b>				
GAT	9.36	7.89	6.64	5.32
Conv+GAT	10.05	9.07	7.17	6.15
GAT+U-Net	8.39	7.49	6.60	5.66
GAT+U-Net**	13.34	12.07	<b>11.46</b>	<b>9.62</b>
Conv+GAT+U-Net	8.31	7.47	6.66	5.15
Conv+GAT+U-Net**	<b>13.43</b>	<b>12.52</b>	11.43	9.55

Table D.5: Large Scale Experiment: GAT-Denoiser components vs. baseline algorithms.

## D.5 Large Scale Experiments: Visual Results

In this section, further visual results for the large scale experiment are presented for  $\text{SNR}_y$  0 dB, -5 dB, -10 dB and -15 dB. Clean images are repeated at every subsection, even though they are the same.

### D.5.1 $\text{SNR}_y$ 0 dB

#### D.5.1.1 Clean Test Images

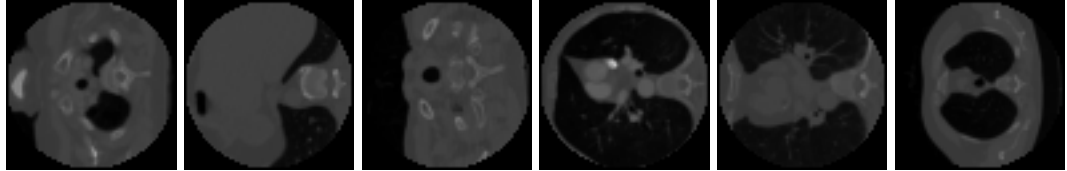


Figure D.1: Clean samples.

#### D.5.1.2 Baseline Algorithms

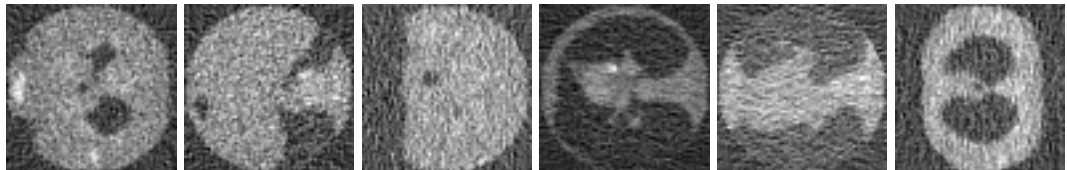


Figure D.2: FBP reconstruction for  $\text{SNR}_y$  0 dB.

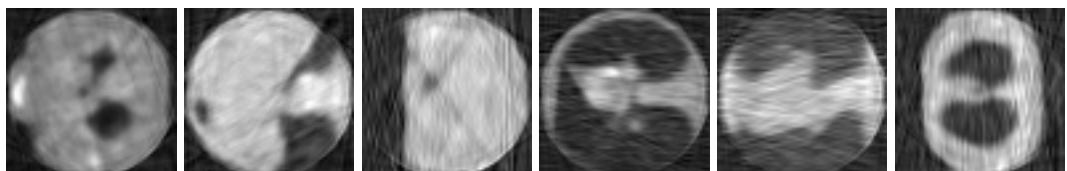


Figure D.3: BM3D sino reconstruction for  $\text{SNR}_y$  0 dB.

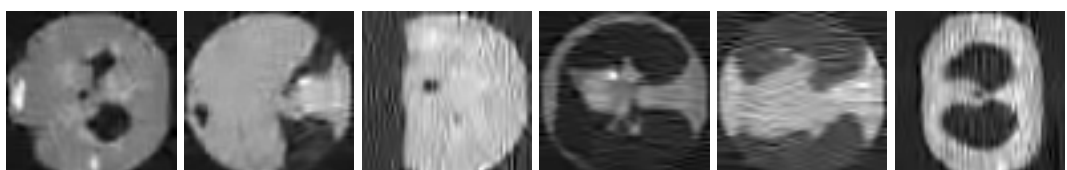


Figure D.4: BM3D reco reconstruction for  $\text{SNR}_y$  0 dB.

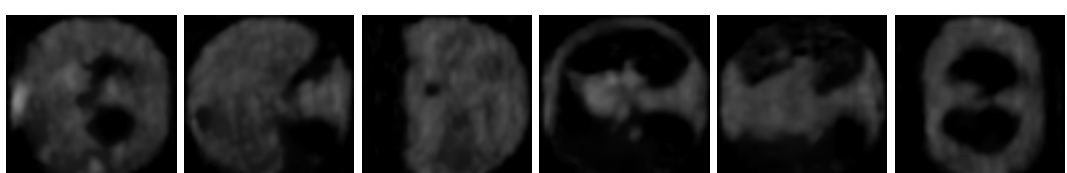


Figure D.5: U-Net reconstruction for  $\text{SNR}_y$  0 dB.

### D.5.1.3 GAT-Denoiser Models

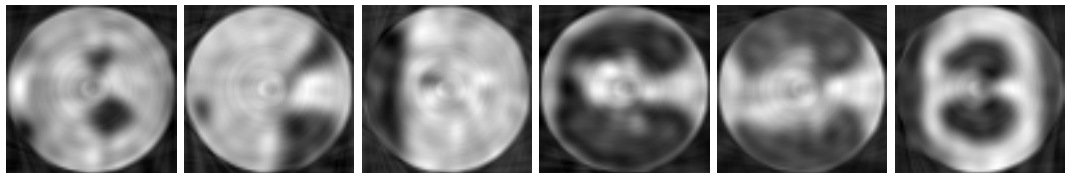


Figure D.6: GAT reconstruction for  $\text{SNR}_y$  0 dB.

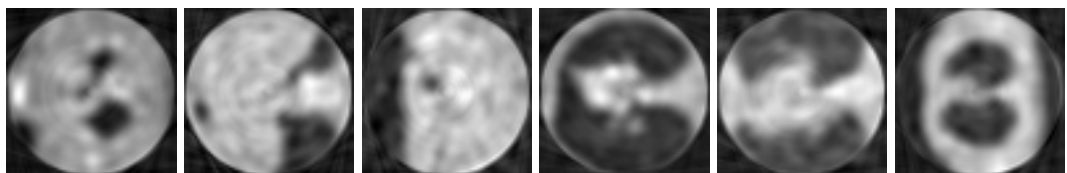


Figure D.7: Conv + GAT reconstruction for  $\text{SNR}_y$  0 dB.

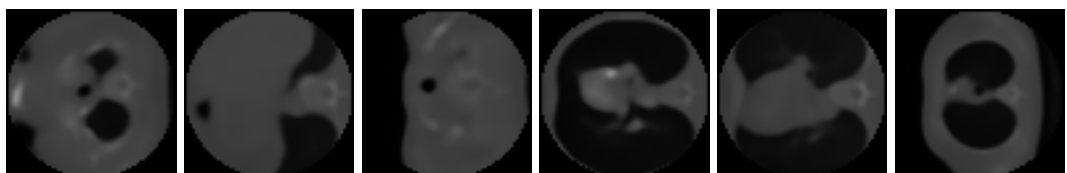


Figure D.8: GAT + U-Net reconstruction for  $\text{SNR}_y$  0 dB.

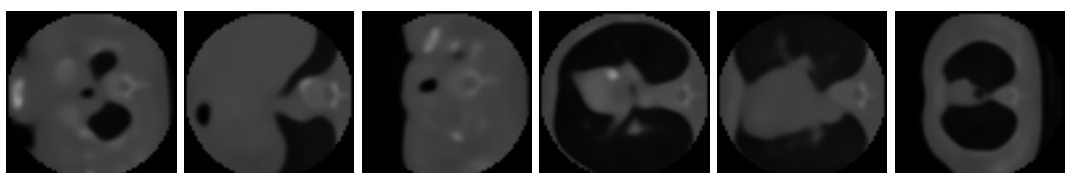


Figure D.9: Conv + GAT + U-Net reconstruction for  $\text{SNR}_y$  0 dB.

### D.5.2 $\text{SNR}_y$ -5 dB

#### D.5.2.1 Clean Test Images

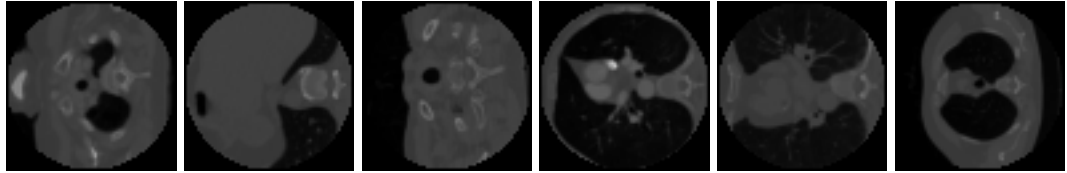


Figure D.10: Clean samples.

#### D.5.2.2 Baseline Algorithms

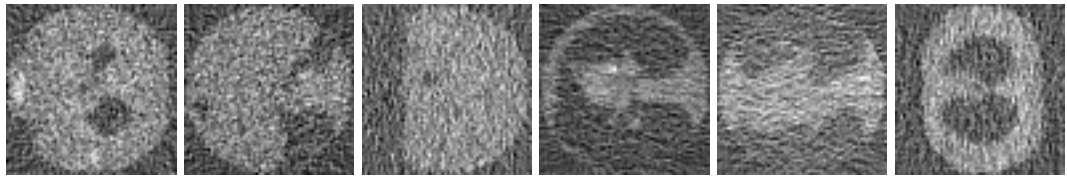


Figure D.11: FBP reconstruction for  $\text{SNR}_y$  -5 dB.

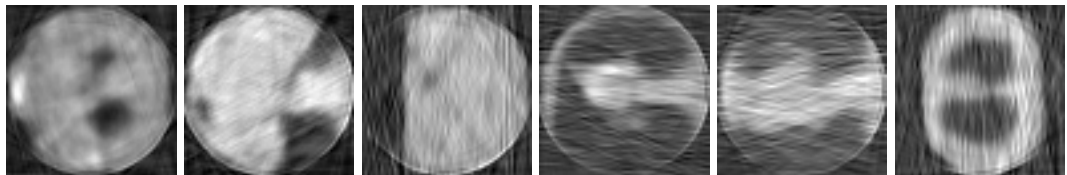


Figure D.12: BM3D sino reconstruction for  $\text{SNR}_y$  -5 dB.

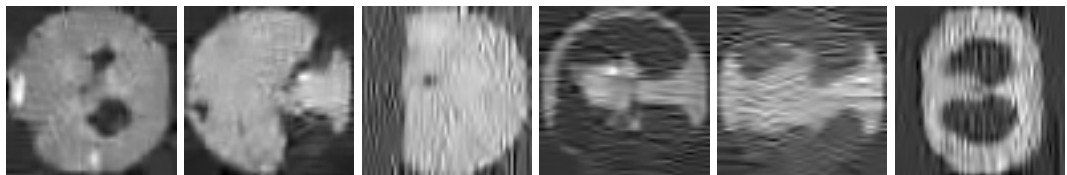


Figure D.13: BM3D reco reconstruction for  $\text{SNR}_y$  -5 dB.

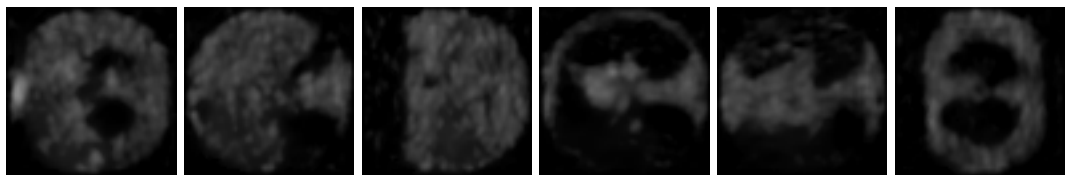


Figure D.14: U-Net reconstruction for  $\text{SNR}_y$  -5 dB.

### D.5.2.3 GAT-Denoiser Models

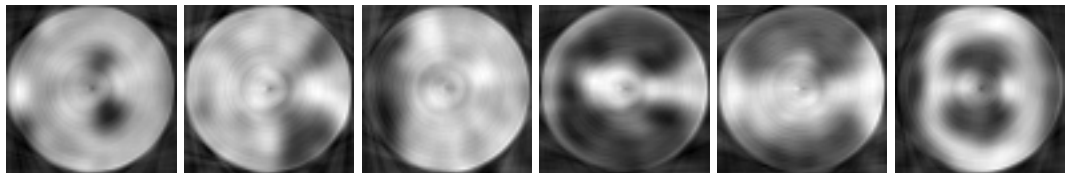


Figure D.15: GAT reconstruction for  $\text{SNR}_y = -5 \text{ dB}$ .

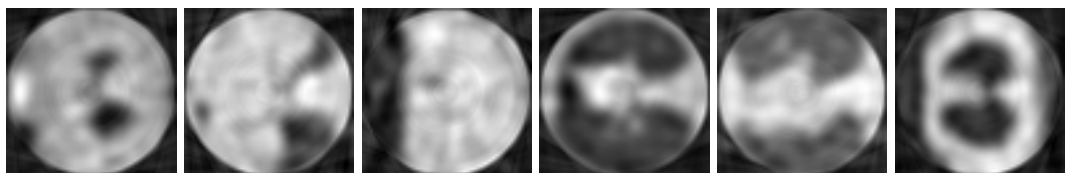


Figure D.16: Conv + GAT reconstruction for  $\text{SNR}_y = -5 \text{ dB}$ .

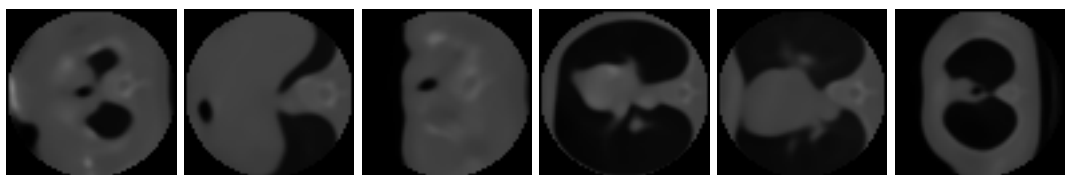


Figure D.17: GAT + U-Net reconstruction for  $\text{SNR}_y = -5 \text{ dB}$ .

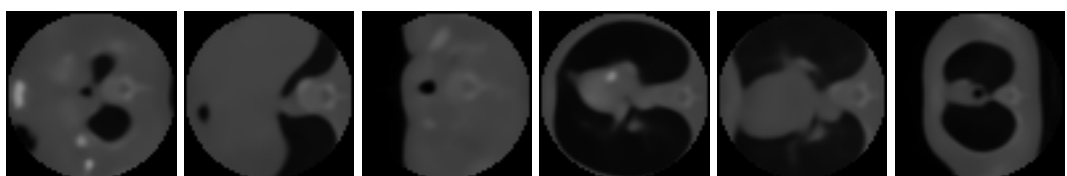


Figure D.18: Conv + GAT + U-Net reconstruction for  $\text{SNR}_y = -5 \text{ dB}$ .

### D.5.3 $\text{SNR}_y$ -10 dB

#### D.5.3.1 Clean Test Images

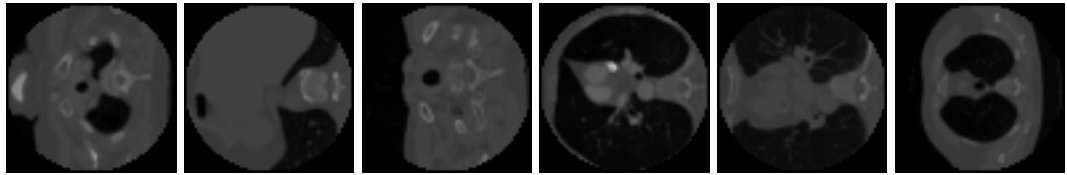


Figure D.19: Clean samples.

#### D.5.3.2 Baseline Algorithms

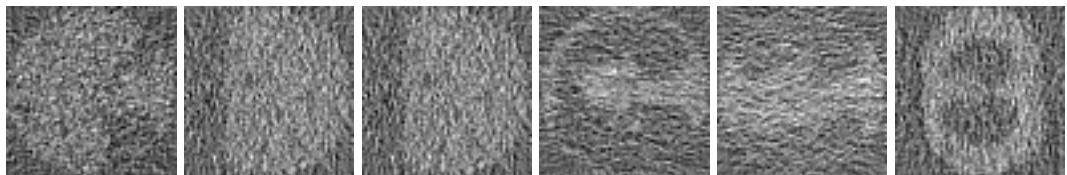


Figure D.20: FBP reconstruction for  $\text{SNR}_y$  -10 dB.

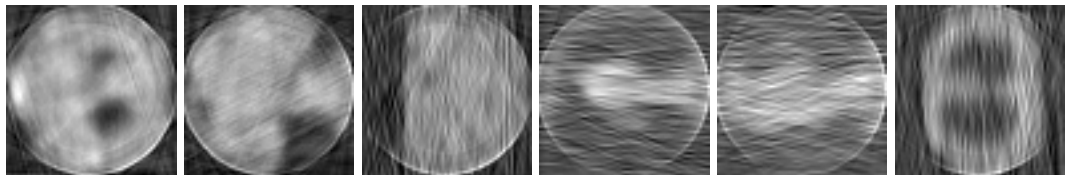


Figure D.21: BM3D sino reconstruction for  $\text{SNR}_y$  -10 dB.

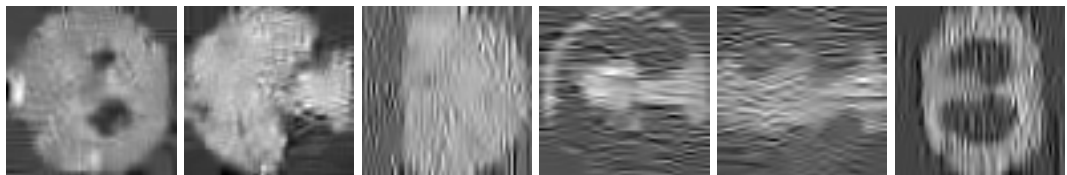


Figure D.22: BM3D reco reconstruction for  $\text{SNR}_y$  -10 dB.

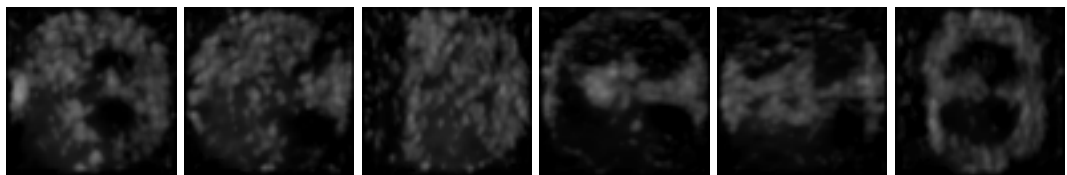


Figure D.23: U-Net reconstruction for  $\text{SNR}_y$  -10 dB.

### D.5.3.3 GAT-Denoiser Models

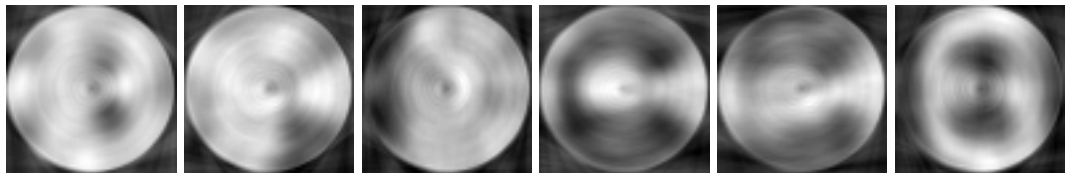


Figure D.24: GAT reconstruction for  $\text{SNR}_y$  -10 dB.

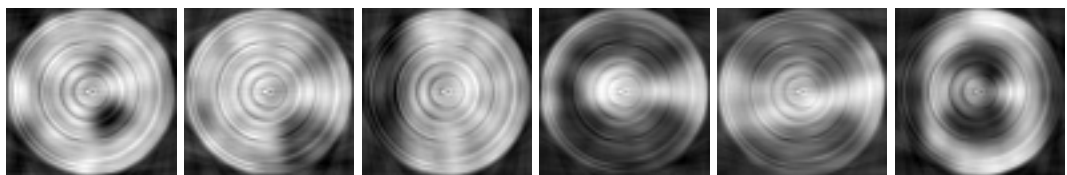


Figure D.25: Conv + GAT reconstruction for  $\text{SNR}_y$  -10 dB.

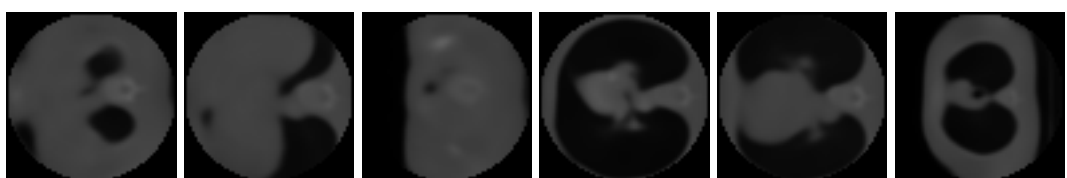


Figure D.26: GAT + U-Net reconstruction for  $\text{SNR}_y$  -10 dB.

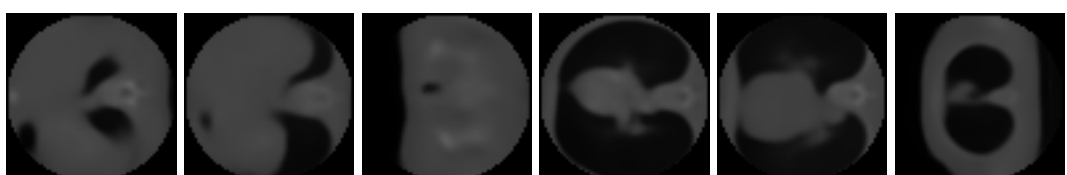


Figure D.27: Conv + GAT + U-Net reconstruction for  $\text{SNR}_y$  -10 dB.

#### D.5.4 $\text{SNR}_y$ -15 dB

##### D.5.4.1 Clean Test Images

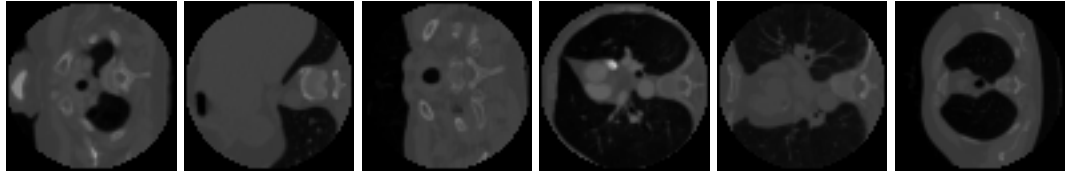


Figure D.28: Clean samples.

##### D.5.4.2 Baseline Algorithms

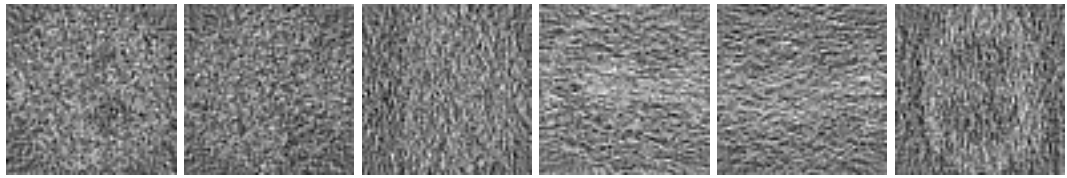


Figure D.29: FBP reconstruction for  $\text{SNR}_y$  -15 dB.

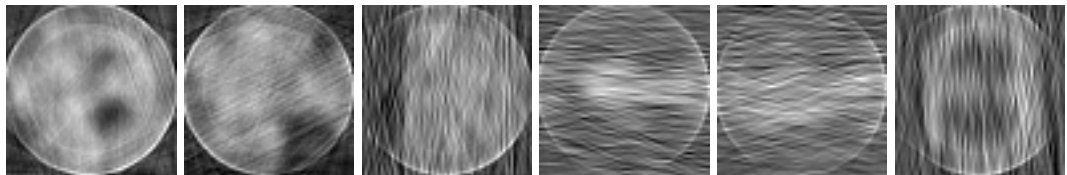


Figure D.30: BM3D sino reconstruction for  $\text{SNR}_y$  -15 dB.

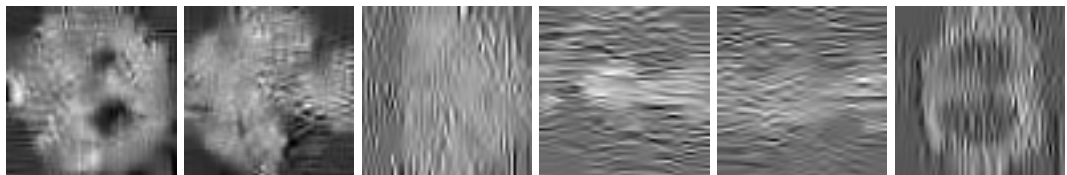


Figure D.31: BM3D reco reconstruction for  $\text{SNR}_y$  -15 dB.

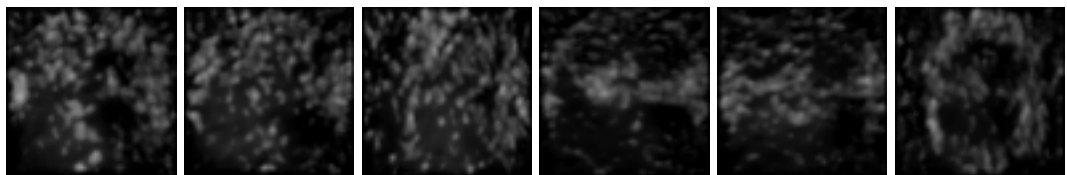


Figure D.32: U-Net reconstruction for  $\text{SNR}_y$  -15 dB.

#### D.5.4.3 GAT-Denoiser Models

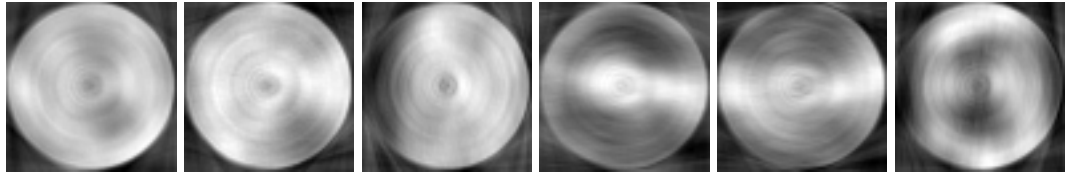


Figure D.33: GAT reconstruction for  $\text{SNR}_y$  -15 dB.

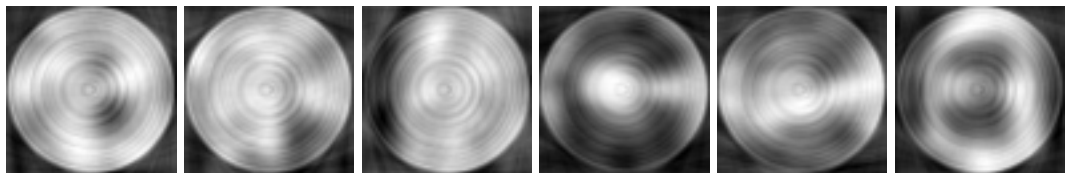


Figure D.34: Conv + GAT reconstruction for  $\text{SNR}_y$  -15 dB.

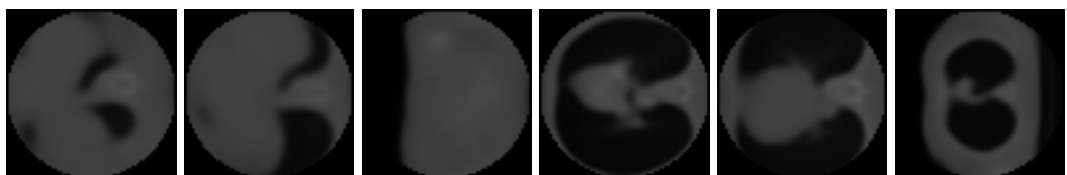


Figure D.35: GAT + U-Net reconstruction for  $\text{SNR}_y$  -15 dB.

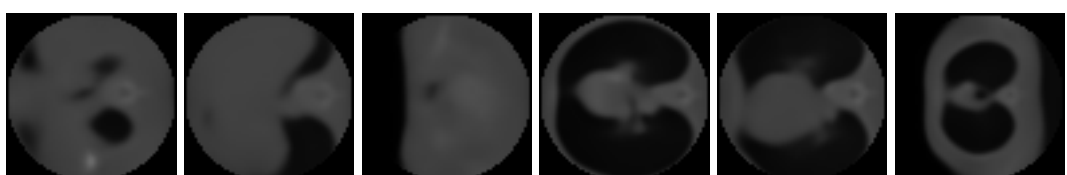


Figure D.36: Conv + GAT + U-Net reconstruction for  $\text{SNR}_y$  -15 dB.

## D.6 Wandb Results

Table D.6 shows urls raw wandb results for all computed experiments on the LoDoPaB-CT dataset.

Experiments	URL
<b>Small Scale Experiments:</b>	
FBP	<a href="https://wandb.ai/cedric-mendelin/FBP-Validation-LoDoPaB-small">https://wandb.ai/cedric-mendelin/FBP-Validation-LoDoPaB-small</a>
BM3D	<a href="https://wandb.ai/cedric-mendelin/BM3D-Validation-LoDoPaB-small">https://wandb.ai/cedric-mendelin/BM3D-Validation-LoDoPaB-small</a>
U-Net	<a href="https://wandb.ai/cedric-mendelin/U-Net-Validation-LoDoPaB-small">https://wandb.ai/cedric-mendelin/U-Net-Validation-LoDoPaB-small</a>
K-nn	<a href="https://wandb.ai/cedric-mendelin/LoDoPaB-Small-k-NN-and-graph-size">https://wandb.ai/cedric-mendelin/LoDoPaB-Small-k-NN-and-graph-size</a>
Convolution	<a href="https://wandb.ai/cedric-mendelin/LoDoPaB-Small-Convolution">https://wandb.ai/cedric-mendelin/LoDoPaB-Small-Convolution</a>
Loss	<a href="https://wandb.ai/cedric-mendelin/LoDoPaB-Small-Loss-FBP-vs-SINO">https://wandb.ai/cedric-mendelin/LoDoPaB-Small-Loss-FBP-vs-SINO</a>
GAT dropout	<a href="https://wandb.ai/cedric-mendelin/LoDoPaB-Small-GAT-dropout">https://wandb.ai/cedric-mendelin/LoDoPaB-Small-GAT-dropout</a>
GAT-Denoiser $k = 2$	<a href="https://wandb.ai/cedric-mendelin/LoDoPaB-Small-Components-knn-2">https://wandb.ai/cedric-mendelin/LoDoPaB-Small-Components-knn-2</a>
GAT-Denoiser $k = 8$	<a href="https://wandb.ai/cedric-mendelin/LoDoPaB-Small-Components-knn-8">https://wandb.ai/cedric-mendelin/LoDoPaB-Small-Components-knn-8</a>
<b>Large Scale Experiments:</b>	
U-NET	<a href="https://wandb.ai/cedric-mendelin/U-Net-Validation-LoDoPaB-large">https://wandb.ai/cedric-mendelin/U-Net-Validation-LoDoPaB-large</a>
FBP	<a href="https://wandb.ai/cedric-mendelin/FBP-Validation-LoDoPaB-large">https://wandb.ai/cedric-mendelin/FBP-Validation-LoDoPaB-large</a>
BM3D	<a href="https://wandb.ai/cedric-mendelin/BM3D-Validation-LoDoPaB-large">https://wandb.ai/cedric-mendelin/BM3D-Validation-LoDoPaB-large</a>
GAT-Denoiser	<a href="https://wandb.ai/cedric-mendelin/LoDoPaB-Large-knn-2">https://wandb.ai/cedric-mendelin/LoDoPaB-Large-knn-2</a>

Table D.6: Wandb raw results.

**Average Wandb Run Result:** Average SNR and loss have been computed with a python script and exported values can be found under<sup>13</sup>.

<sup>13</sup> [https://github.com/cedricmendelin/master-thesis/tree/main/wandb\\_results](https://github.com/cedricmendelin/master-thesis/tree/main/wandb_results)



## **Declaration on Scientific Integrity**

(including a Declaration on Plagiarism and Fraud)

Translation from German original

Title of Thesis:

Name Assesor: Prof. Dr. Ivan Dokmanić  
Name Student: Cédric Mendelin  
Matriculation No.: 2014-469-274

With my signature I declare that this submission is my own work and that I have fully acknowledged the assistance received in completing this work and that it contains no material that has not been formally acknowledged. I have mentioned all source materials used and have cited these in accordance with recognised scientific rules.

Place, Date: Therwil, 9.6.2022 Student: 

Will this work be published?

No

Yes. With my signature I confirm that I agree to a publication of the work (print/digital) in the library, on the research database of the University of Basel and/or on the document server of the department. Likewise, I agree to the bibliographic reference in the catalog SLSP (Swiss Library Service Platform). (cross out as applicable)

Publication as of: 12.06.2022

Place, Date: Therwil, 9.6.2022 Student: 

Place, Date: \_\_\_\_\_ Assessor: \_\_\_\_\_

*Please enclose a completed and signed copy of this declaration in your Bachelor's or Master's thesis .*